Journal of Asian Earth Sciences 272 (2024) 106244

Contents lists available at ScienceDirect

Journal of Asian Earth Sciences

journal homepage: www.elsevier.com/locate/jseaes

Using compositions of zircon to reveal fertile magmas for the formation of porphyry deposits in the Loei and Truong Son fold belts, northern Laos

Peerapong Sritangsirikul[a,*], Sebastien Meffre[a], Khin Zaw[a], Ivan Belousov[a], Yi-Jen Lai[b], Alex Richards[c], Punya Charusiri[d]

[a] CODES Centre of Ore Deposit and Earth Sciences, University of Tasmania, Hobart, Tasmania 7001, Australia
[b] Macquarie Geoanalytical, the Macquarie Analytical and Fabrication Facility (MAFF), Macquarie University, Sydney, New South Wales 2109, Australia
[c] Rio Tinto Exploration, Brisbane, Queensland 4001, Australia
[d] Morphology of Earth Surface and Advance Geohazards in Southeast Asia Research Unit (MESA RU), Department of Geology, Faculty of Science, Chulalongkorn University, Bangkok 10400, Thailand

ARTICLE INFO

Keywords:
Loei fold belt
Truong Son fold belt
Zircon
Geochronology
Trace elements
Porphyry-related fertility

ABSTRACT

The Loei and Truong Son fold belts are well known as being the most geologically important and highly mineralized magmatic arc-related terranes in mainland southeast Asia. Numerous studies have examined the geology, geochemistry, and geochronology but only a few metallogenic and detailed deposit characterizations have been undertaken. This study of zircon geochemical analyses uses laser ablation inductively coupled plasma mass spectrometry (LA-ICP-MS) to provide U-Pb ages and magmatic fertility of felsic to intermediate volcanic and plutonic rocks from ten prospects in the Loei and Truong Son fold belts, in the northwest Laos region. The geochemical and geochronological analyses suggest at least three episodes of magmatism occurred: Silurian-Devonian (434–411 Ma), Early to Middle Permian (299–277 Ma), and Late Permian to Middle Triassic (253–243 Ma). The variable ranges of εHf values (−12 to + 12) suggest that mantle-derived and crustal contamination signatures are related to the history of subduction and arc magmatism in this region. Key trace elements and ratios associated with oxygen fugacity of magmas (e.g., Eu/Eu*, Dy/Yb, Ce/Nd, ΔFMQ) imply that the Phu Kham and the west of Vientiane along the Mekong River are likely to be fertile for porphyry copper deposits. In contrast, the Pha Gnai and other suites are less fertile. Using zircon as a fertility indication can be a valuable tool to distinguish between fertile and barren magmatic suites in this area.

1. Introduction

The Loei (Loei-Phetchabun) Fold Belt (LFB) and the Truong Son Fold Belt (TSFB) are the most critical, highly mineralized volcano-magmatic arcs in mainland southeast Asia. The LFB lies to the east of the Sukhothai Fold Belt and the Nan-Uttarradit Suture, at the western margin of the Indochina Terrane, while the TSFB lies along the northeastern margin of the Indochina Terrane (Fig. 1). Although the geologically distinct and economically important rocks of the Loei and Truong Son fold belts have been well studied, there has been little discussion of the nature of the magmatism and mineral potential of the belts in many southeast Asian tectonic reconstructions (Gardiner et al., 2015, 2016a, 2016b, 2017; Morley et al., 2011; Sone and Metcalfe, 2008). New studies in north-western Laos are providing valuable geological, geochemical, and geochronological constraints in the northern part of the TSFB (Blanchard et al., 2013; Burrett et al., 2021; Qian et al., 2015, 2016a, 2016b; Rossignol et al., 2016; Shi et al., 2021; Wang et al., 2016, 2020; Zhang et al., 2020) however, only a few metallogenic and detailed deposit studies have been completed.

Zircon chemical composition has been utilized in mineralized fold belts worldwide to discriminate mineralized fertile magmas from pre-mineralization magmas and provide insights into the complex petrogenesis that resulted in a low-temperature, hydrous and oxidized fertile magma composition for porphyry deposit exploration (Ballard et al., 2002; Bouzari and Hart, 2019; Dilles et al., 2015; Hart et al., 2017; Lee et al., 2021; Leslie et al., 2022; Loader et al., 2017; Loucks et al., 2020; Lu et al., 2016; Rezeau et al., 2019; Shen et al., 2015; Shu et al., 2019; Zou et al., 2019). This paper uses these techniques to investigate the

* Corresponding author.
E-mail addresses: peerapong.sritangsirikul@utas.edu.au (P. Sritangsirikul), sebastien.meffre@utas.edu.au (S. Meffre), ivan.belousov@utas.edu.au (I. Belousov), yi-jen.lai@mq.edu.au (Y.-J. Lai), alex.richards@riotinto.com (A. Richards), punya.c@chula.ac.th (P. Charusiri).

https://doi.org/10.1016/j.jseaes.2024.106244
Received 19 December 2023; Received in revised form 30 June 2024; Accepted 1 July 2024
Available online 4 July 2024

petrogenesis of mineralized magmatic and volcanic rocks from known deposits and prospective sites, mainly in northern Laos, by documenting the key trace element ratios in zircons (e.g., Eu/Eu*, (Ce/Nd)/Yb, Gd/Yb and Hf). These data are compared to identify the mineralized versus barren magmas, highlighting the importance of zircon trace element data for the investigation of mineral fertility in the study area.

2. Geological background

The southeast Asia region comprises several micro-tectonic terranes including, from west to east, Sibumasu, Inthanon Suture Zone, Sukhothai Terrane, and the Indochina Terrane. These terranes were amalgamated during a complex tectonic history involving subduction, back-arc rifting, and collisions (Burrett et al., 2021, 2014; Gardiner et al.,

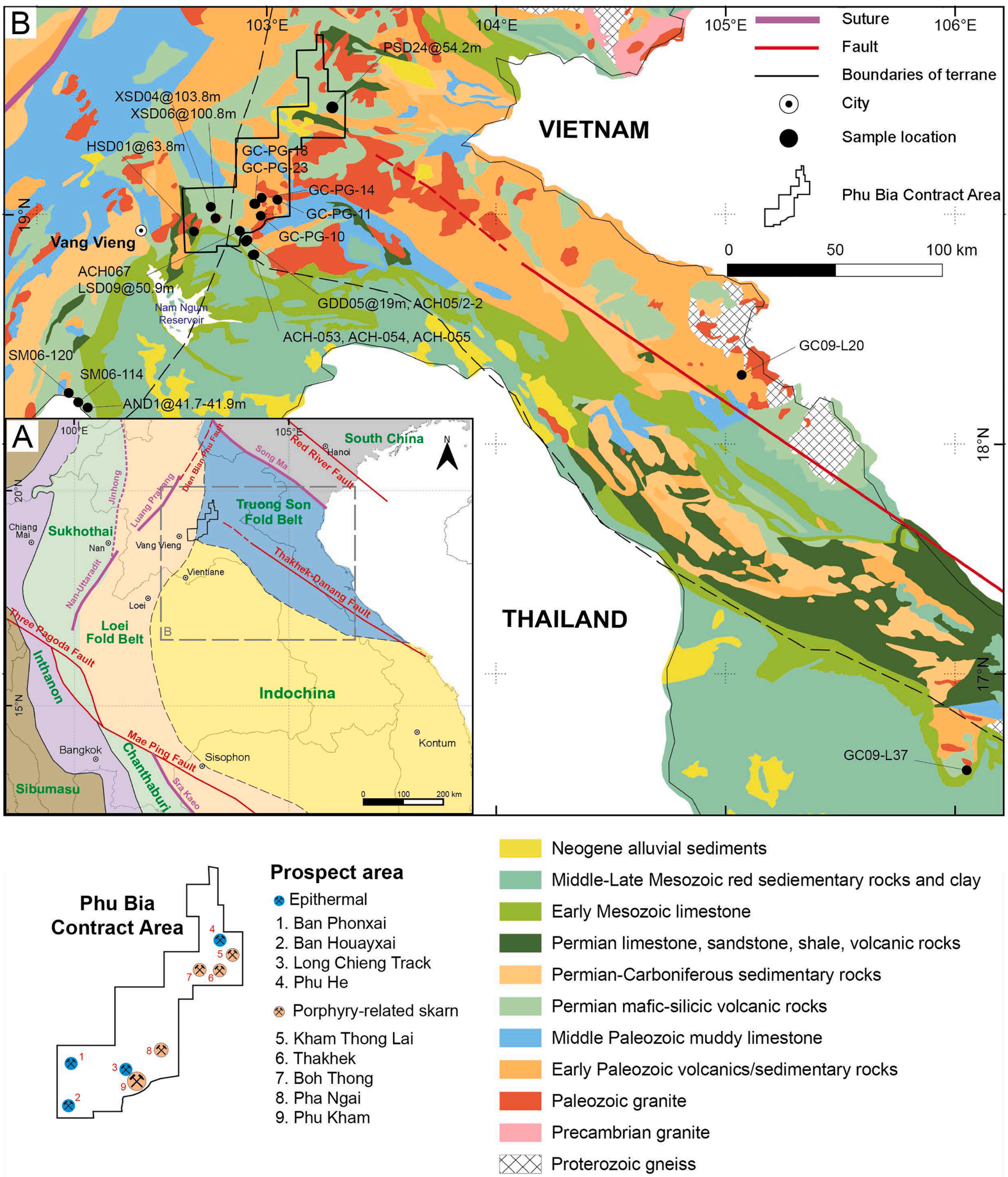

Fig. 1. A) Regional tectonic map of mainland Southeast Asia (modified after Khin Zaw et al., 2014; Wang et al., 2016; Shi et al., 2020). B) Simplified geological map of the Northwest Laos region modified from the British Geological Survey (1990) and Leaman et al. (2019).

2017; Khin Zaw et al., 2014; Metcalfe, 2011a, 2011b, 2013; Shi et al., 2021; Sone and Metcalfe, 2008; Wang et al., 2016, 2018, 2020a, 2020b, 2023). The Indochina Terrane rifted from Gondwana during the opening of the Paleo-Tethys Ocean in the Paleozoic. This terrane comprises several microcontinental segments including the Kontum Massif, Truong Son Fold Belt and Loei Fold Belt (Burrett et al., 2021, 2014; Metcalfe, 2011b, 2013; Khin Zaw et al., 2014). This study examines both the age and the potential for intrusive rocks in the Loei and Truong Son Fold Belts to host porphyry Cu-Au deposits.

2.1. Truong Son Fold Belt

The Truong Son Fold Belt (TSFB) lies along the northeastern margin of the Indochina Terrane which contains mainly Paleozoic marine volcanic and sedimentary rocks, including the Ordovician-Silurian arc-related volcanics and granitoids, Ordovician-Silurian siliciclastics with minor limestone, and widespread Devonian carbonates (Burrett et al., 2021). The fold belt is bounded to the southeast by the Tam Ky–Phuoc Son Suture which separates the Truong Son Fold Belt from the highly metamorphosed Kontum Massif in central Vietnam (Khin Zaw et al., 2014). To the southwest the boundary is partially obscured by younger rocks in the Khorat Plateau. To the northwest the Truong Son has an indistinct boundary with the Loei Fold Belt.

The TSFB contains magmatic rocks belonging to five magmatic episodes (Shi et al., 2021; Wang et al., 2020a; Zhang et al., 2020):

1. Ordovician-Silurian volcanic and intrusive rocks (465–427 Ma).
2. Late Carboniferous-Early Permian (330—280 Ma) subduction-related volcanic and intrusive rocks are associated with porphyry-related Cu-Au skarn, and epithermal Cu-Au deposits.
3. Early Permian-Mid Triassic (280–240 Ma) rocks are associated with calc-alkaline porphyry Cu-Au deposits.
4. Middle-Late Triassic volcanic and intrusive rocks.
5. Cretaceous granitoids.

The TSFB contains world-class porphyry-related skarn-type Cu-Au deposits, e.g., Phu Kham (Kamvong, 2013; Kamvong et al., 2014), epithermal Au deposits (e.g., Ban Houayxai (Manaka et al., 2014), subvolcanic mesothermal Au deposits (e.g., Long Chieng Track (Leaman et al., 2019; Manaka, 2008), sediment-hosted Au deposits (e.g., Sepon (Cromie, 2010; Cromie et al., 2018, 2006) and orogenic gold deposits (Bounliyong et al., 2022).

2.2. Loei Fold Belt

The Loei Fold Belt (LFB) marks the margin between the Indochina and Sukhothai terranes by the Nan-Sra Kaeo Suture, which is generally regarded as a short-lived Permian back-arc basin (e.g., Sone and Metcalfe, 2008). The LFB forms as an N-S trending arcuate magmatic-volcanic arc extending from Luang Prabang in northern Laos, Loei and Phetchabun in Thailand, and Sra Kaeo in southeastern Thailand and into western Cambodia and eastern Shan State in Myanmar (Hu et al., 2022; Khin Zaw, 2021; Khin Zaw et al., 2022b, 2022a).

The LFB contains mainly Late Permian to Triassic andesitic–rhyolitic volcanic rocks, with the center covered by the thick Mesozoic Khorat 'red beds' on the Khorat Plateau. Ordovician, Silurian to Devonian–Carboniferous magmatic rocks, Devonian to Lower Carboniferous siliciclastic and volcaniclastic rocks and minor radiolarian cherts and limestones are also reported (Burrett et al., 2021; Hunyek et al., 2020; Khin Zaw et al., 2014; Qian et al., 2021; Shi et al., 2021).

The Triassic LFB granitoids were previously regarded as S-type, e.g. Sone and Metcalfe (2008) and Morley et al. (2011). However, geochemical studies reveal that most of the granitoids are in fact I-type, consistent with the abundance of copper–gold mineralization in the belt (Khin Zaw et al., 2007, 2014, 2022a, 2022b, 2021; Khin Zaw et al., 2009). The LFB hosts several major porphyry-related copper–gold skarns and epithermal gold deposits, such as the Chatree deposits in Thailand. The porphyry-related skarn-type Cu-Au deposits (Puthep; PUT1 and PUT2, Phu Thap Fah, Phu Lon, French Mine) occur in fractures and veins typically centered on dioritic to granodioritic intrusions (Kamvong et al., 2014; Khin Zaw et al., 2014; Khin Zaw and Meffre, 2007; Salam, 2013; Salam et al., 2014). Recently orogenic gold deposits, e.g., Phapon old deposit (Guo et al., 2019) and stratabound Cu–Pb–Ag deposits, e.g., Ban Kiouchep (Zhang et al., 2020; Zou et al., 2020) were also recorded. In the Chatree district, the Carboniferous rocks of the LFB are dominated by limestone and volcanogenic sedimentary rocks. Rhyolitic siltstone near Wang Pong has yielded a U-Pb zircon age of 327 ± 7 Ma (Khin Zaw and Meffre, 2007; Salam, 2013). In general, the interbedded sequences of the Carboniferous limestone with siltstone and sandstone crop out mainly as small exposures. Thicker sequences of interbedded siltstone and fine-grained sandstone occurs on the west of Dong Khui (Salam, 2013). Late Carboniferous hornblende granite intruded the Carboniferous limestone, which caused the local metamorphism to marble (310 ± 8 Ma: U-Pb zircon: Khin Zaw and Meffre, 2007). The Middle Permian limestone bodies occur as thick sequences overlying the Carboniferous sedimentary rocks marked by basal conglomerate, siltstone, and shale (Salam, 2013; Salam et al., 2014).

3. Analytical methods

3.1. Sample acquisition

The samples used for this study were collected in Laos and Thailand during industry and Australian Research Council (ARC)-funded research (Khin Zaw and Meffre, 2007) on the LFB and TSFB carried out between 2004–2014 (see Table S1, Appendix A). Although many of the ages of the magmatic rocks and zircons had been analyzed, trace element compositions and Hf isotopes from the zircon crystals had not been acquired, so information on the potential for the rocks to host porphyry deposits was not available.

The samples selected for this study come from several Cu-Au and Au deposits and prospect areas in Laos, including;

1) An area west of Vientiane along the Mekong,
2) the Ang Noi Prospect,
3) the Ban Nape Prospect,
4) the Ban Houayxai Deposit,
5) the Long Chieng Track Deposit,
6) the Phu Kham Deposit,
7) the Ban Phonxai Deposit,
8) the Nhon Nhang Prospect,
9) the Phu He Prospect,
10) the Pha Gnai Prospect (see Fig. 1 and Table 1 for more details).

The samples selected for this study were either: 1) granitic rocks including granite, diorite, and gneissic granite (or orthogneiss), quartz, K-feldspar, and plagioclase with minor muscovite, biotite, and hornblende or 2) intermediate to felsic porphyritic magmatic rocks with 4–8 mm feldspar phenocrysts (>10 %) in very fine-grained or microcrystalline quartz and plagioclase. The lithological details are provided in Table S1, Appendix A.

The whole-rock geochemistry of the samples was analyzed during the previous projects (Khin Zaw and Meffre, 2007) and are provided in Table S2, Appendix A and summarized in Figs. 2 and 3.

3.2. Zircon U-Pb and Hf isotopic analyses

Twenty-one zircon mounts (Table 1) were analyzed using Agilent 7900 quadrupole ICPMS at CODES (Utas), coupled to a COMPex Pro 110 excimer laser operating at 193 nm wavelength and equipped with an ASI S155 laser ablation cell capable of holding 20 1-inch size grain mounts. The analysis was performed at least one hour after the ignition of the

Table 1
Summary of the samples analyzed in this study.

No	Sample	Locality	Lithology	Latitude	Longitude	U-Pb Age ± 2σ (Ma)
1	AND1@41.7–41.9 *m*	Ang Noi Au Prospect	Chlorite-altered granite	18.159	102.220	420 ± 3
2	HSD01@63.8 *m*	Ban Houayxai Au Deposit	Andesite	18.926	102.684	287 ± 2
3	GC09-L20	Ban Nape Prospect	Porphyritic granite	18.301	105.069	253 ± 2
4	XSD04@103.8 *m*	Ban Phonxai Prospect	Rhyodacite	19.033	102.756	279 ± 2
5	XSD06@100.8 *m*	Ban Phonxai Prospect	Andesitic basalt	18.984	102.777	289 ± 2
6	LSD09 @ 50.9 *m*	Long Chieng Track (LCT) Au Deposit	Dacite	18.928	102.882	277 ± 3
7	ACH067	Long Chieng Track (LCT) Au Deposit	Feld-phyric rhyolite	18.929	102.882	292 ± 2
8	ACH05/2–2	Long Chieng Track (LCT) Au Deposit	Foliated granite	18.889	102.915	424 ± 5
9	GC09-L37	Nhon Nhang Prospect	Orthogneiss	16.581	106.050	244 ± 3
14	GC-PG-10	Pha Gnai Prospect	Granite	18.999	102.966	287 ± 2
13	GC-PG-11	Pha Gnai Prospect	Diorite	19.064	103.047	285 ± 1
12	GC-PG-14	Pha Gnai Prospect	Diorite	19.073	102.979	273 ± 2
10	GC-PG-18	Pha Gnai Prospect	Rhyolite	19.047	102.950	267 ± 2
11	GC-PG-23	Pha Gnai Prospect	Rhyolite	19.047	102.946	273 ± 2
15	PSD24@54.2 *m*	Phu He Prospect	Quartz rhyolite	19.465	103.281	284 ± 3
16	GDD05@19 *m*	Phu Kham Cu-Au Deposit	Dacite	18.883	102.908	300 ± 2
17	ACH053	Phu Kham Cu-Au Deposit	Porphyritic granite	18.826	102.946	422 ± 4
18	ACH054	Phu Kham Cu-Au Deposit	Muscovite granite	18.826	102.945	411 ± 4
19	ACH055	Phu Kham Cu-Au Deposit	Biotite-Muscovite granite	18.824	102.939	425 ± 3
20	SM06-114	West of Vientiane along Mekong River	Quartz diorite	18.183	102.178	244 ± 2
21	SM06-120	West of Vientiane along Mekong	Quartz-feldspar rhyolite	18.223	102.137	435 ± 2

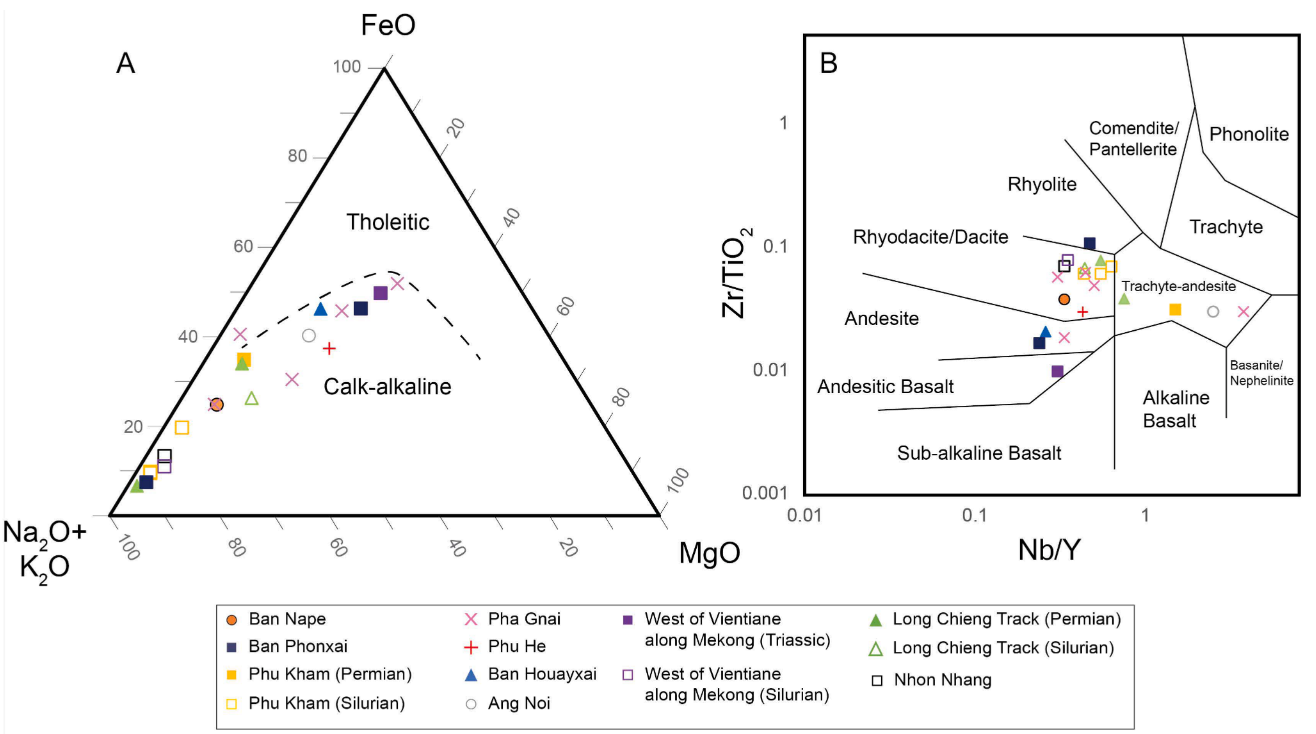

Fig. 2. Whole-rock geochemistry plots showing the geochemical variations of different magmatic suites in the LFB and TSFB; A) $Na_2O + K_2O$-FeO-MgO ternary plot (Modified from Irvine and Baragar, 1971) and B) Zr/TiO_2 vs Nb/Y diagram (Winchester and Floyd, 1977).

mass spectrometer to stabilize the machine. Primary and secondary zircon standards were analyzed at the beginning, the end, and throughout the analytical run. The downhole fractionation, instrument drift, and mass bias correction factors for Pb/U ratios on zircons were calculated using analyses on the primary standard (91500; Wiedenbeck et al., 1995) and checked on secondary standards (Temora, from Black et al., 2003) and Plešovice from Sláma et al., 2008). The $^{207}Pb/^{206}Pb$ ratio was calibrated using analyses on NIST610. The zircons were analyzed with a laser beam at 29 μm spots at 5 Hz and approximately 2 J/cm^2 laser fluence. The 30-second gas blank was analyzed at the beginning of each measurement and followed by 30 s of ablation. The ablation was performed in He atmosphere flowing at 0.35 L/min and mixed with Ar straight after ablation flowing at 1.05 L/min. Each element was measured successively every 0.253 s and recorded for data reduction. Isotopic masses collected were ^{31}P, ^{49}Ti, ^{56}Fe, ^{89}Y, ^{91}Zr, ^{93}Nb, ^{139}La, ^{140}Ce, ^{141}Pr, ^{146}Nd, ^{147}Sm, ^{153}Eu, ^{157}Gd, ^{159}Tb, ^{163}Dy, ^{165}Ho, ^{166}Er, ^{169}Tm, ^{172}Yb, ^{175}Lu, ^{178}Hf, ^{181}Ta, ^{202}Hg, ^{204}Pb, ^{206}Pb, ^{207}Pb, ^{208}Pb, ^{232}Th, ^{235}U and ^{238}U. The U/Pb geochronology data reduction was conducted using the LADR software program. Data were reported on an Excel spreadsheet using ISOPLOT4.15 (Ludwig, 2012) to generate Concordia diagrams, probability density plots and age calculations. Cathodoluminescence (CL) imaging techniques were obtained and employed to document zircon grain structure at the Central Science Laboratory (Utas), using the FEI MLA650 scanning electron microscope (SEM). The CL images were the basis for locating and determining the options for LA-ICP-MS and Hf isotope analytical sites.

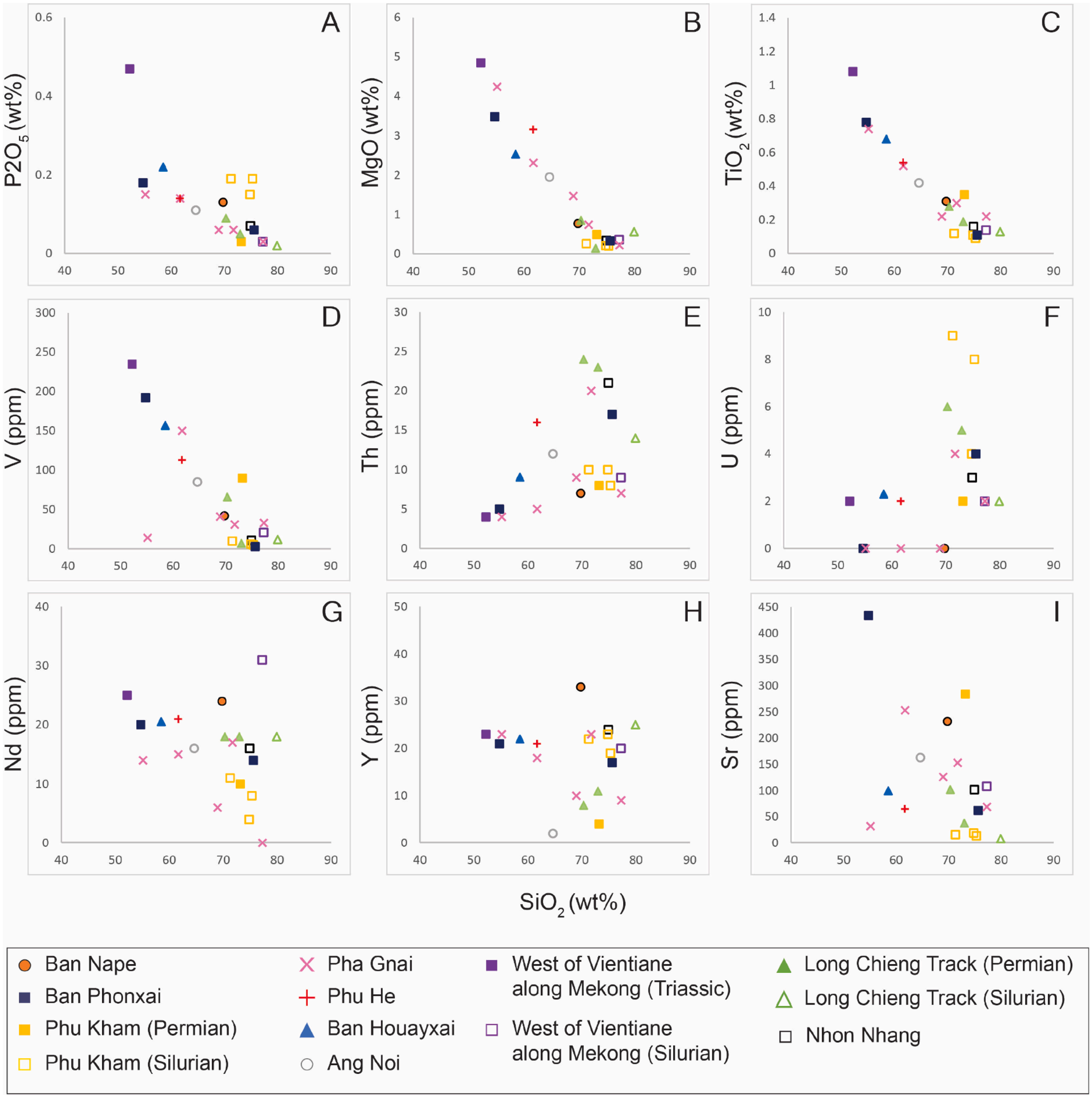

Fig. 3. Whole-rock geochemistry bivariate diagrams of major and trace elements versus SiO_2 A) P_2O_5, B) MgO, C) TiO_2, D) V (ppm), E) Th (ppm), F) U (ppm), G) Nd (ppm), H) Y (ppm), and Sr (ppm).

After U-Pb analysis, the zircon mounts were sent to Macquarie GeoAnalytical, (Macquarie University), for Hf isotope analyses using the Teledyne Photon Machines LSX-213 G2 + laser-ablation system, attached to a Nu Plasma II multi-collector inductively coupled plasma mass spectrometer (LA-MC-ICPMS). The analyses targeted either the same or the nearest spot from which the U-Pb isotope and trace element data were obtained. The analytical techniques are described in detail by Griffin et al. (2004) and Maritati et al. (2019). The analyses began with 30 s of blank gas followed by ablation at 5 Hz and 3 J/cm^2 for 60 s with a beam diameter of approximately 30–50 μm (depending on the size of the zircon grain). To ensure that Hf isotope analyses were contained within the same domain analyzed for U-Pb, the zircon CL images were used to correlate the location. Two analytical sessions were conducted for each sample measurement. Zircons from the Mud Tank carbonatite locality were analyzed together with the samples in each session to monitor the accuracy of the results. The mean $^{176}Hf/^{177}Hf$ value and most of the data are within two standard deviations of the recommended value (0.282522 ± 42 (2σ); Griffin et al., 2006). Temora zircon was run as an independent check on the accuracy of the Yb correction. The average $^{176}Hf/^{177}Hf$ ratio for Temora is consistent with the published value for the Temora standard (0.282687 ± 24 (2σ); Hawkesworth and Kemp, 2006). The initial $^{176}Hf/^{177}Hf$ (Hf_i) value in zircon is calculated using the measured $^{176}Hf/^{177}Hf$ and apparent $^{207}Pb/^{206}Pb$ age. Calculation of εHf_i values employed the decay constant of Scherer et al. (2001) of 1.865 x 10^{-11}. A complete tabulation of zircon Hf isotopic data of the samples from this study and standard is presented in Appendix C.

The Eu anomaly [Eu/Eu*] was calculated using Sm and Gd (Eu_n/(Sm_n x Gd_n)$^{1/2}$). The Ce anomaly [Ce/Ce*] can be calculated by Ce_n / (La_n x Pr_n)$^{1/2}$. However, La in zircon is difficult to measure and the Ce/Ce* and Ce/Nd ratio was used to define the zircon Ce anomaly (Chelle-Michou et al., 2014; Loader et al., 2017; Xie et al., 2023).

4. Results

4.1. Zircon u-pb geochronology and Hf isotopic data

The results for U-Pb and Hf isotopic data and CL images for the zircons from the LFB and TSFB are presented below. Further information and U-Pb concordia diagrams are shown in Figs. 2-7 and supplementary materials are found in Table S3-S12, Appendix B.

4.1.1. West of Vientiane along the Mekong River

Forty analyses were analyzed from two zircon mounts of quartz diorite (SM06-114) and quartz-feldspar phyric rhyolite (SM06-120) (see composition details Table S3, Appendix B). Zircons from quartz diorite are mostly subhedral with a length of 60–120 µm. They show a dominantly dark core with a thin, light rim (Fig. 4A). 21 zircons had high U and Th content, of 141–2162 ppm and 101–5450 ppm, respectively. The Th/U ratio is very high (>1). The youngest population of 10 analyses gave the Concordia intercept age of 243.8 ± 1.7 Ma with mean standard weighted deviation (MSWD = 0.99), and a secondary population of nine spots gave an older Concordia intercept age of 252.4 ± 1.8 Ma (Fig. 5A). Zircons from the rhyolite are euhedral with a length of 80–150 µm and show clear oscillatory zoning (Fig. 4A). Nineteen analyses were performed on zircons from the rhyolite. These had low U and Th contents (191–1648 ppm and 114–848 ppm) with a low Th-U ratio (0.38–0.67). The youngest population gave the Concordia intercept age of 434.9 ± 2.0 Ma. (Fig. 5B) Six widely scattered older analyses were found (up to 485 Ma). Hf isotopic analyses were conducted on four magmatic zircons from quartz diorite (SM06-114) and nine magmatic zircons from quartz-feldspar phyric rhyolite (SM06-120) (Table S13, Appendix C). The initial $^{176}Hf/^{177}Hf$ ratios of zircons from quartz diorite range between 0.282791 and 0.282892 with initial εHf values ranging from + 5.1 to + 8.5 (average $\varepsilon Hf_{(t)}$ = +6.5), while the quartz-feldspar phyric rhyolite yielded slight lower values of the initial $^{176}Hf/^{177}Hf$ ratios between 0.282551 and 0.282714, with the initial εHf values ranging from + 0.6 to + 6.5 (average $\varepsilon Hf_{(t)}$ = +3.8; Fig. 10).

4.1.2. Ang Noi

Zircons from the intensely chlorite-altered granite (AND1@41.7–41.9 m) are euhedral small, long prismatic crystals with oscillatory zoning (Fig. 4B). Some crystals contain high U content showing as a dark area in the CL images. Analyses were obtained from 15 zircons with high U (131–907 ppm) and Th (54–987 ppm) with a high Th/U ratio (Table S4, Appendix B). The youngest population (eight analyses) gave the Concordia intercept age of 419.9 ± 3.1 Ma, with an MSWD of 1.3. Five analyses of the secondary population gave the Concordia age of 433.4 ± 3.6 Ma, with an MSWD of 1.5. Two older analyses are also present (465.7 ± 2.6 Ma and 474.7 ± 2.6 Ma; Fig. 5C). Hf isotopes were not analyzed in the zircons from the Ang Noi Au prospect.

4.1.3. Ban Nape

Zircons from the granite of Ban Nape (GC09-L20) are large (100–250 µm) and euhedral. The oscillatory zoning is very clear in the rims around an older core (Fig. 4C). A total of 48 analyses resulted in three age populations (Table S5, Appendix B). The eleven youngest analyses gave a weighted mean $^{206}Pb/^{238}U$ age of 252.5 ± 1.6 Ma (MSWD = 1.6; Fig. 5D) with older populations at 257.7 ± 1.0 Ma (MSWD = 1.1, n = 13) and 264.6 ± 2.4 Ma (MSWD = 1.4, n = 9). The analyses of eleven zircons for Hf isotopes yielded initial $^{176}Hf/^{177}Hf$ ratios ranging from 0.282175 to 0.282372, with initial εHf values ranging from −9.3 to −17.0 (average $\varepsilon Hf_{(t)}$ = -11.0; Fig. 10, Table S13).

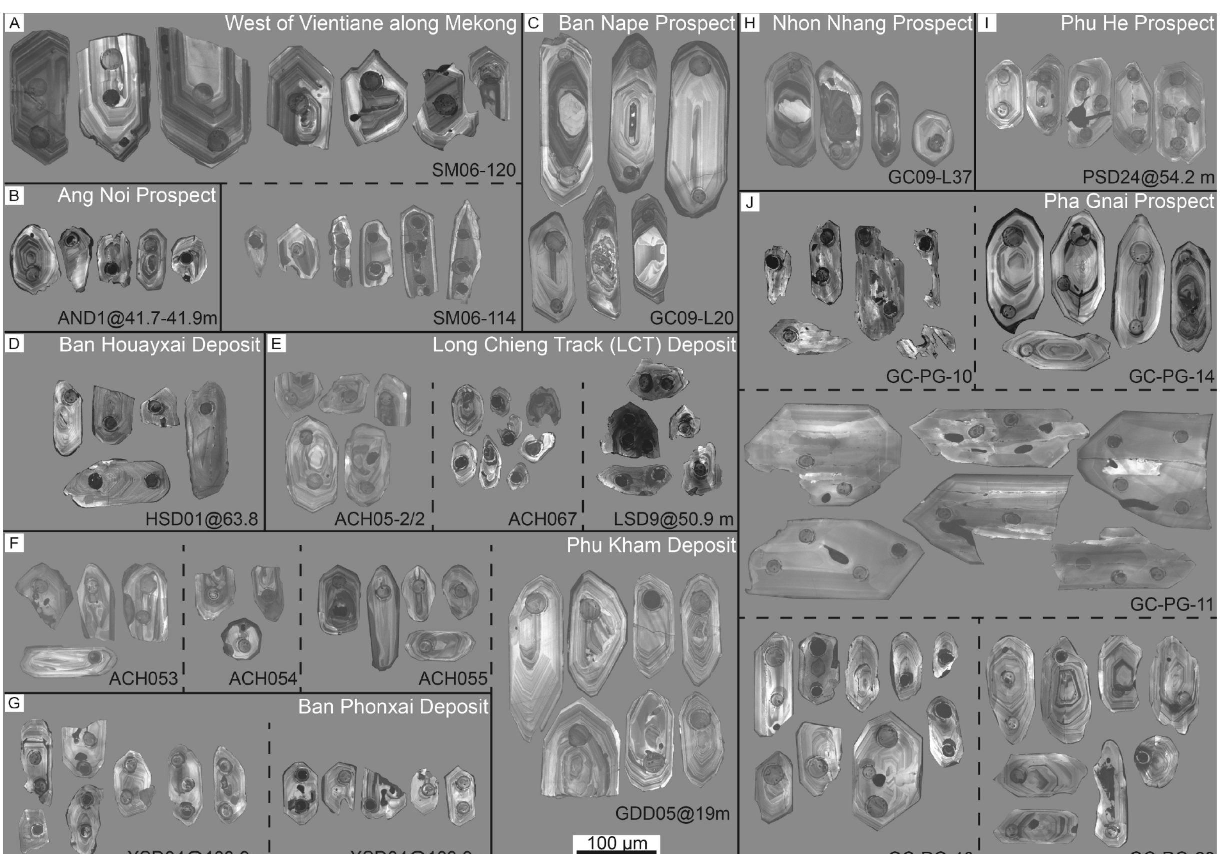

Fig. 4. Representative cathodoluminescence images of analyzed zircons from Laos. The CL images show variations in size and internal structure of zircons investigated in this study. A) West of Vientiane along Mekong, B) Ang Noi Prospect, C) Ban Nape Prospect, D) Ban Houayxai Deposit, E) Long Chieng Track Deposit, F) Phu Kham Deposit, G Ban Phonxai Deposit, H) Nhon Nhang Prospect, I) Phu He Prospect, and J) Pha Gnai Prospect.

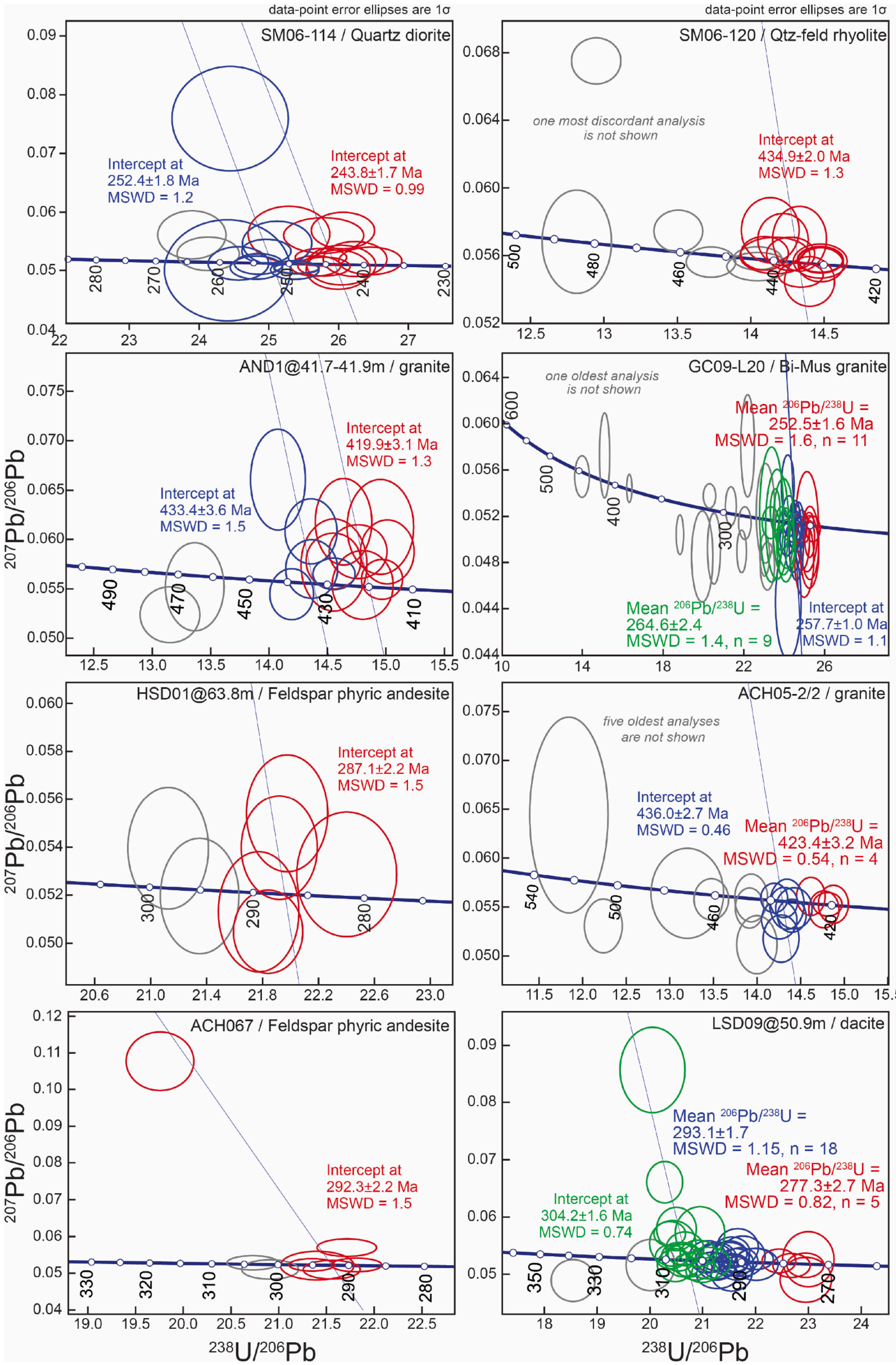

Fig. 5. U–Pb Concordia isotopic age data for representative samples from the magmatic rocks in the study area. (A-B) West of Vientiane along the Mekong River.I) Ang Noi Au Prospect. (D) Ban Nape ProspeI (E) Ban Houayxai Au deposit. (F-H) Long Chieng Track deposit. Datapoint error ellipses are 1σ.

4.1.4. *Ban Houayxai*

Feldspar-phyric andesite (HSD01@63.8 m) from Ban Houayxai Au deposit contains small subhedral-euhedral zircons (40–80 μm) with diffuse oscillatory zoning (Fig. 4D). Seven zircons were analyzed (Table S6) and were characterized by a high concentration of Th (122–405 ppm) and U (276–604 ppm) with a high ratio of Th/U (0.44–0.67). Five of seven analyses gave the single population Concordia intercept age of 287.1 ± 2.2 Ma, with MSWD of 1.5. Two slightly older zircon grains of 295 and 297 Ma are also present (Fig. 5E). Four magmatic zircons were analyzed for Hf isotopes (Table S13). The initial $^{176}Hf/^{177}Hf$ ratios ranged from 0.282424 to 0.282560, with initial εHf values ranging from −1.8 to −6.7 (average $\varepsilon Hf_{(t)}$ = -3.3; Fig. 10).

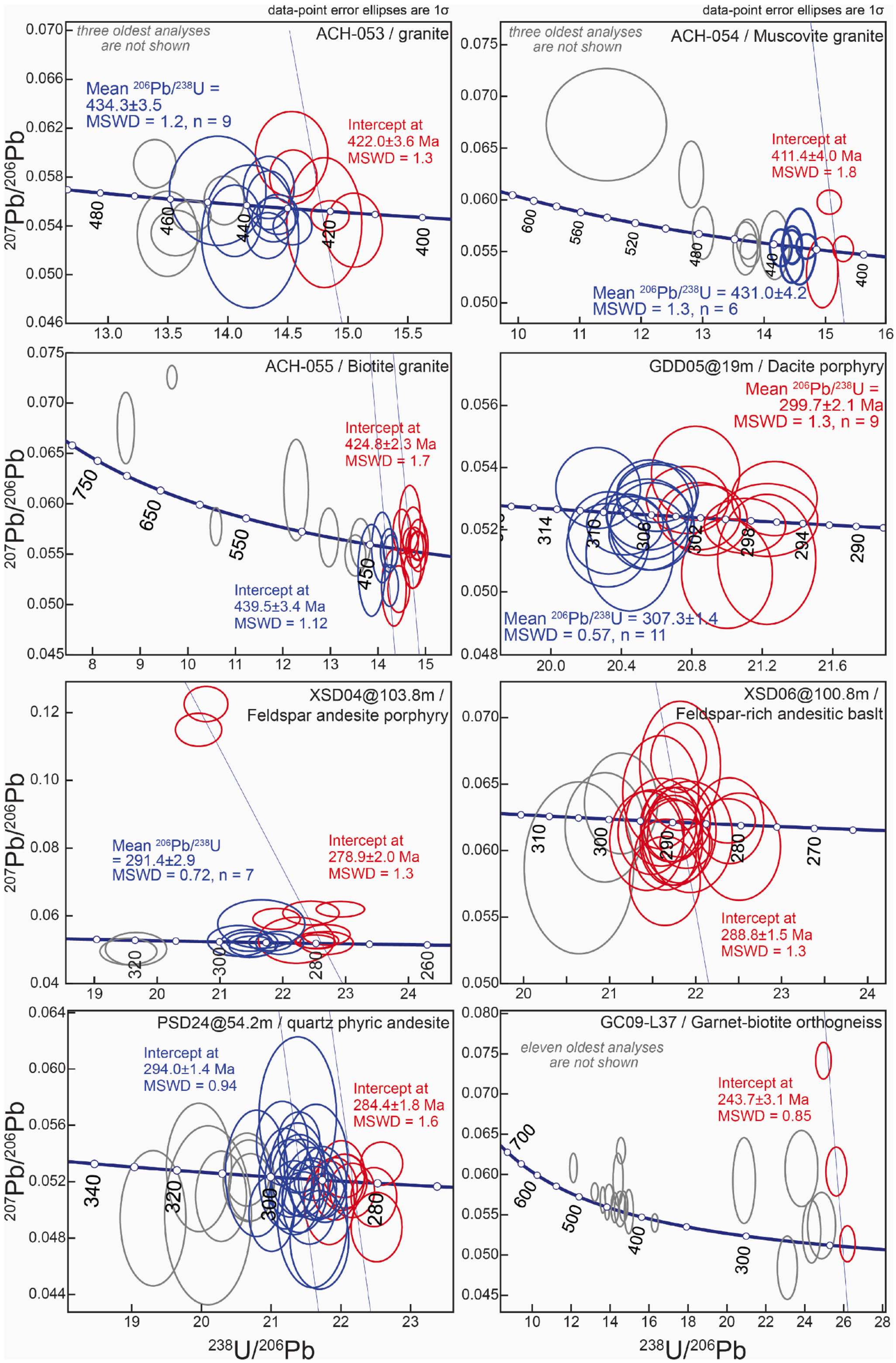

Fig. 6. U–Pb Concordia isotopic age data for representative samples from the magmatic rocks in the study (A-D) Phu Kham (E-F) Ban Phonxai. (G) Phu He. (H) Nhon Nhang. Datapoint error ellipses are 1σ.

4.1.5. *Long Chieng Track*

Three samples of the Long Chieng Track (LCT) deposit area were selected and U-Pb age data are shown in Fig. 3F-H (U-Pb composition details are shown in Table S7, Appendix B). The first is foliated granite (ACH05-2/2), with a primarily small euhedral grain of twenty-three zircons with sector and oscillatory zoning (Fig. 4E), and the four youngest analyses gave a weighted mean age of 423.4 ± 3.2 Ma (Fig. 5F). However, seven grains yielded a weighted mean age of 436.0 ± 2.7 Ma. The second sample is feldspar-phyric rhyolite porphyry (ACH067). Ten zircons were analyzed, giving a Concordia intercept age of 292.3 ± 2.2 Ma (MSWD = 1.5; Fig. 5G), with two spots excluded due to common Pb and Pb loss issues. Zircons from ACH067 are smaller than

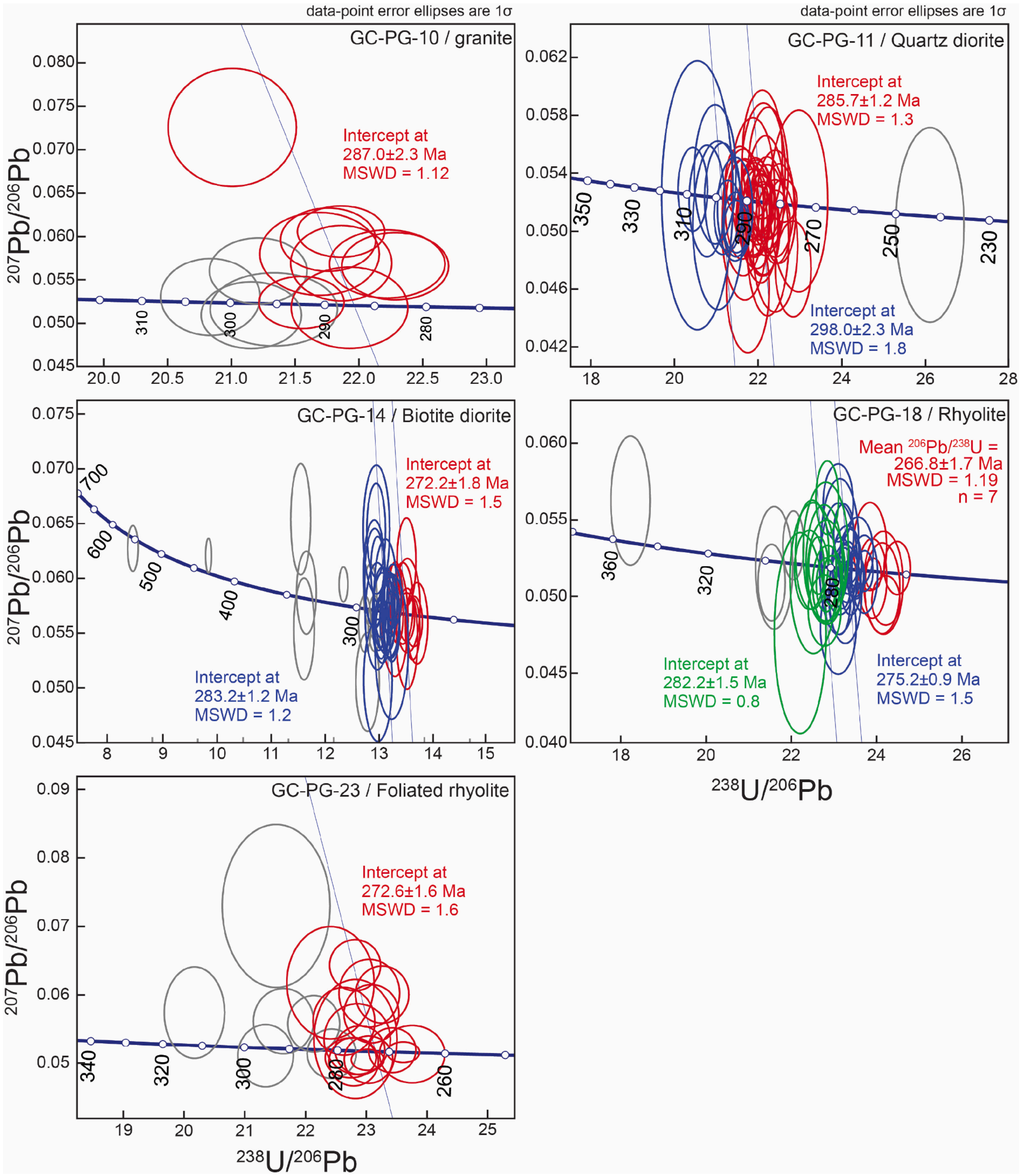

Fig. 7. U–Pb Concordia isotopic age data for representative samples from the magmatic rocks in the study area. (A-E) Pha Gnai Prospect. Datapoint error ellipses are 1σ.

ACH05-2/2 showing eroded rim and oscillatory zoning. The third sample is dacite (LSD09@50 m) containing small euhedral zircons with high U contents (Fig. 4E). Forty-two spots were analyzed giving the youngest population of five analyses yielded a weighted mean $^{206}Pb/^{238}U$ age of 277.3 ± 2.7 Ma (Fig. 5H). Other possible populations are at ~ 293.1 Ma (18 analyses) and at ~ 304.2 Ma (17 analyses). Two older analyses are also present (315 and 339 Ma). Nine magmatic zircons of dacite (LSD09@50 m) and rhyolite (ACH067) from LCT were analyzed for Hf isotopes (Table S13, Appendix C). The initial $^{176}Hf/^{177}Hf$ ratios range from 0.282575 to 0.282687, with initial εHf values ranging from −1.7 to −2.5 (average $\varepsilon Hf_{(t)}$ = -1.2; Fig. 10).

4.1.6. Phu Kham

Four samples of granite (ACH-053, −054, −055) and dacite porphyry (GDD05@19 m) were collected from the Phu Kham Au deposit area. One of the Phu Kham samples, ACH05/2–3, was excluded due to possible Pb loss, and other grains display a range of ages with no coherent populations. However, the two youngest grains have an age of 297.8 Ma.

Most crystals are subhedral to euhedral. However, zircons from the dacite porphyry are euhedral and tend to be larger (Fig. 4F) with prominent and multiple oscillatory zones reflecting a complex crystallization history. Sixty-three analyses were performed on zircons from the granites. These have low Th content and variable U content. The

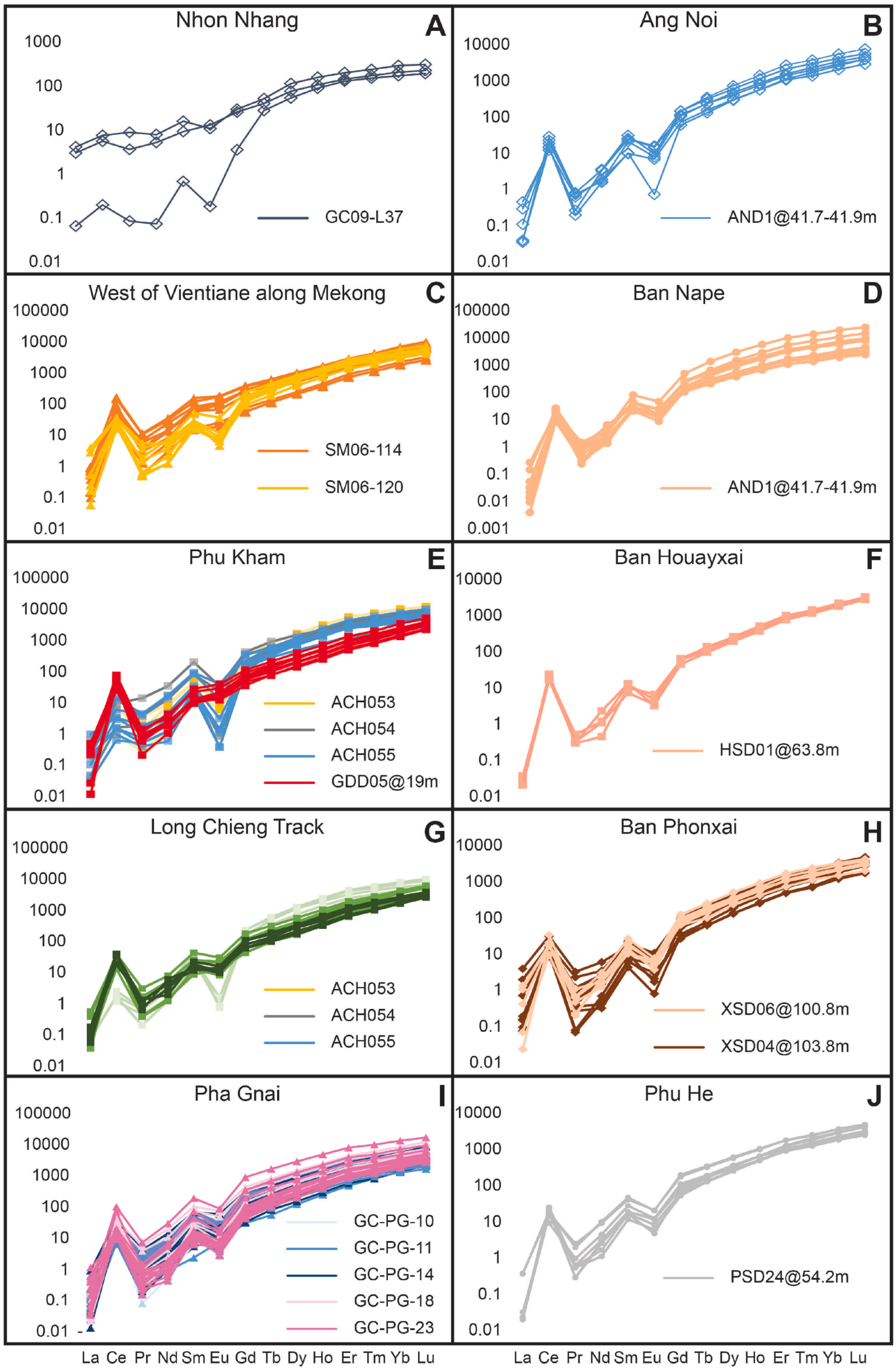

Fig. 8. Chondrite-normalized pattern showing rare earth element distribution of the zircons from different magmatic rocks from the studied area. (A) Nhon Nhang. (B) Ang Noi Au Prospect. (C) West of Vientiane along the Mekong River. (D) BanIpe. (E) Phu Kham Cu-Au skarn deposit. (F) Ban Houayxai Au deposit. (G) Long Chiang Track (LCT) Au deposit. (H) Ban Phonxai Prospect. (I) Pha Gnai Prospect. (J). Phu He Cu-Au skarn Prospect. Normalization values of Sun and McDonough (1989).

youngest populations from each sample gave weighted mean $^{206}Pb/^{238}U$ ages between 411.4 ± 4.0, 422.0 ± 3.6 Ma, and 424.8 ± 3.4 Ma (Fig. 6A-C, Table S8). Twenty spots were analyzed on zircons from sample GDD05@19 m. The nine youngest analyses out of twenty (Fig. 6D) interpreted as the crystallization age of dacite porphyry gave a weighted mean $^{206}Pb/^{238}U$ age of 299.7 ± 2.1 Ma (MSWD = 1.3), and secondary eleven older populations gave the age of 307.3 ± 1.4 (MSWD = 0.57). The nine youngest zircons from Permian dacite porphyry

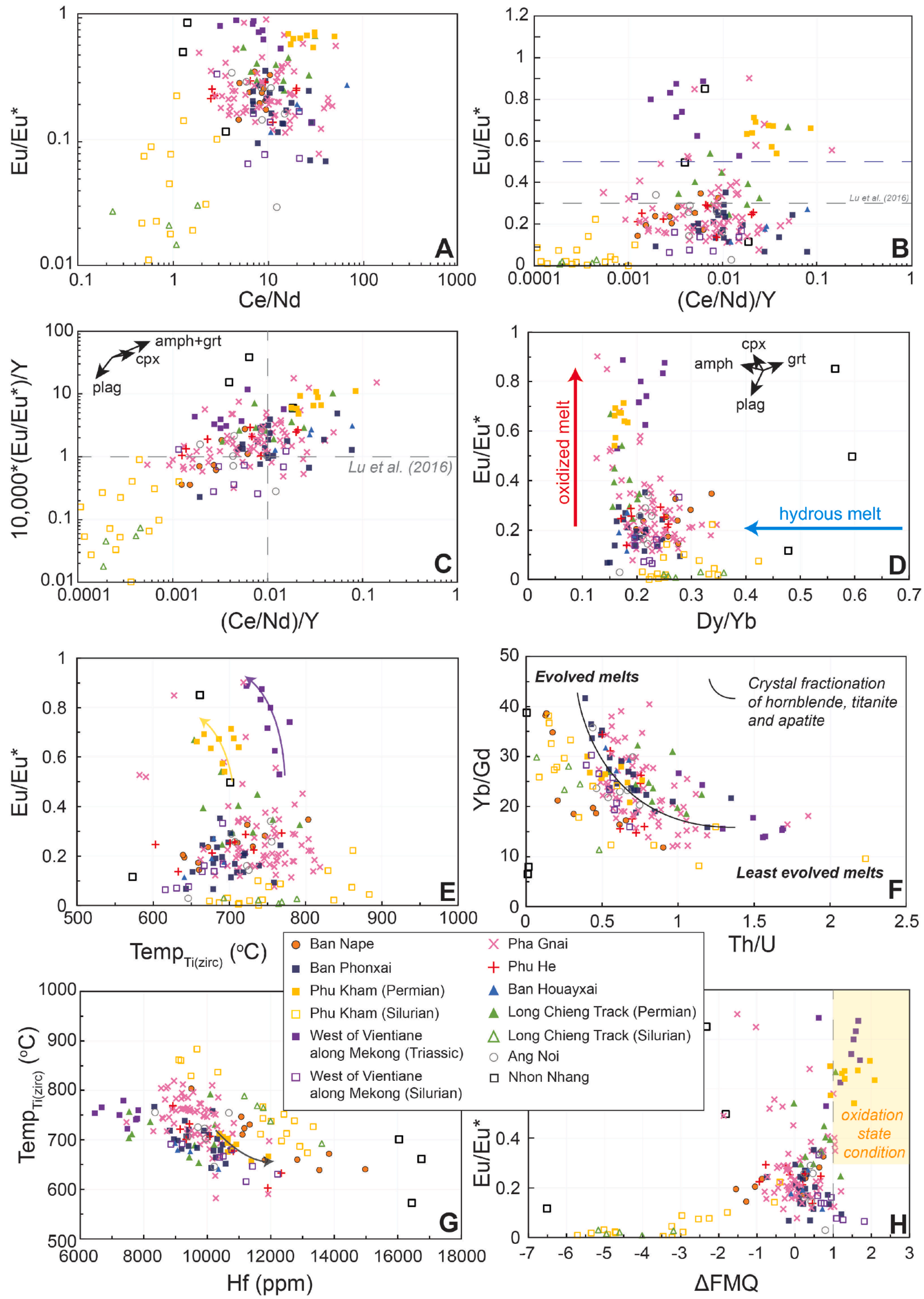

Fig. 9. Zircon trace elements diagrams (after Lu et al., 2016; Leslie et al., 2022 in press) and) showing potential fertility of the magmatic rocks from the studied area. (A) Eu/Eu* vs Ce/Nd. (B) Eu/Eu* vs (Ce/Nd)/Y. (C) 10,000*(Eu/Eu*)/Y vs (Ce/Nd)/Y. (D) Eu/Eu* IDy/Yb. (E) Eu/Eu* vs zircon calculated crystallization temperature. (F) Yb/Gd vs Th/U. (G) zircon calculated crystallization temperature vs Hf contents. (H) Eu/Eu* vs ΔFMQ.

(GDD05@19 m) and eleven zircons from Silurian granites (ACH-054 and ACH-055) were chosen for Hf isotopic analyses (Table S13, Appendix C). The initial $^{176}Hf/^{177}Hf$ ratios of the dacite sample range from 0.282637 to 0.282730, with initial εHf values ranging from 1.2 to 6.5 (average $\varepsilon Hf_{(t)} = 3.9$), whereas the initial $^{176}Hf/^{177}Hf$ ratios of the granites ranging from 0.282271 to 0.282379, with initial εHf values ranging −9.9 to −6.0 (average $\varepsilon Hf_{(t)}$ = -8.2; Fig. 10).

4.1.7. *Ban Phonxai*

Twenty-eight zircons were obtained from rhyolite and dacite porphyry (XSD04@103.8 m and XSD06@100.8 m). They are euhedral, sharp hexagonal prismatic crystals with lengths of 40–70 μm (Fig. 4G).

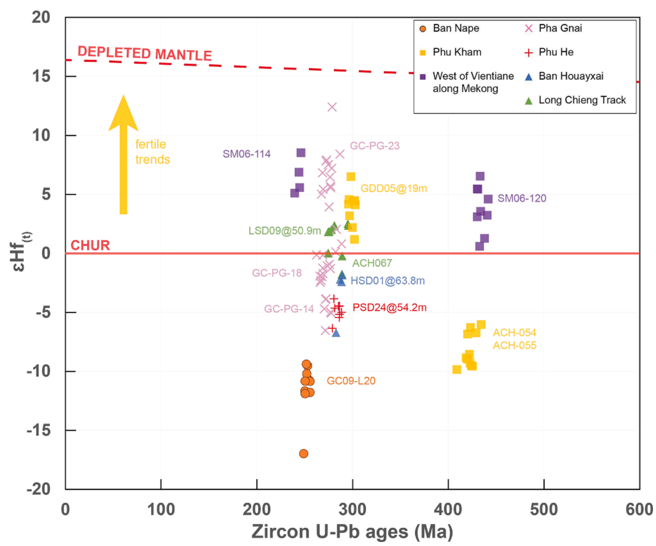

Fig. 10. εHf vs U-Pb zircon ages of analyzed zircons from the LFB and TSFB, Northern Laos region.

The zircons from both samples gave a high concentration of Th and U, which resulted in a high Th/U ratio (0.4–1.3) (Table S9, Appendix B). The ten youngest analyses of rhyolite porphyry gave a Concordia intercept age of 278.9 ± 2.0 Ma (MSWD = 1.3). In comparison, nineteen analyses from dacite porphyry yielded an intercept age of 288.8 ± 1.5 Ma (MSWD = 1.3) (Fig. 6E-F). Hf isotopic analyses were not undertaken on the zircons from the Ban Phonxai Prospect.

4.1.8. Phu He

Zircons from quartz-plagioclase phyric andesite (PSD24@54.2 m) are mostly euhedral small to intermediate crystals of 100–150 μm (Fig. 4I). The nine youngest zircons yielded a weight mean $^{206}Pb/^{238}U$ age of 284.4 ± 2.7 Ma (Table S10) with MSWD of 1.5 and a probability of 0.16 (Fig. 6G). The other possible age population is 294 Ma (20 analyses). Seven older zircons ranging from 304 to 326 Ma are also present. Eight Hf isotopic analyses yielded the initial $^{176}Hf/^{177}Hf$ ratios of this sample ranging from 0.282437 to 0.282507, with initial εHf values ranging −6.3 to −3.8 (average $\varepsilon Hf_{(t)}$ = -4.9; Fig. 10, Table S13).

4.1.9. Nhon Nhang

An orthogneiss from southern Laos (GC09-L37) contains small euhedral zircons with a dark sector at the core of the crystals and lighter oscillatory zoning at the rim (Fig. 4H). Thirty-one spots were analyzed (Table S11, Appendix B), but only three analyses gave a Concordia intercept age of 243.7 ± 3.1 Ma (Fig. 6H), with MSWD of 0.85. The remaining analyses are older recording ages up to 505 Ma. Hf isotopic analyses were not analyzed in the zircons from the Nhon Nhang Prospect.

4.1.10. Pha Gnai

Five samples of granite, diorite, and rhyolite from Pha Gnai Prospect were analyzed (Fig. 7A-E). Zircons from the sample named GC-PG-10 are mostly euhedral (Fig. 4J). The youngest population yielded nine concordant analyses out of 15, giving concordant intercept age of 287.0 ± 2.3 Ma (Fig. 7A, Table S12). Four slightly older zircons were also analyzed (296, 297, 298, and 303 Ma).

Zircons from sample GC-PG-11 are euhedral and larger than the others (200–250 μm; Fig. 4J). The youngest thirty-one out of forty analyses gave a weighted mean $^{206}Pb/^{238}U$ age of 285.4 ± 1.4 Ma with secondary age of 296.4 ± 2.5 Ma (9 analyses; Fig. 7B).

Zircons from GC-PG-14 are large, euhedral, elongated hexagonal crystals, (Fig. 4J). They have clear oscillatory zoning, with some crystals showing an inherited core. The crystals gave a Concordia intercept age of 272.7 ± 1.8 Ma (Fig. 7C; 11 analyses, MSWD = 1.5, probability of fit = 0.12) with a population at 283.2 ± 1.2 Ma (23 analyses, MSWD = 1.2, probability of fit = 0.21).

Zircons from GC-PG-18 are euhedral, elongated, hexagonal and prismatic in shape with prominent oscillatory zoning. The youngest population gave a weight mean age of 266.8 ± 1.7 Ma (MSWD = 1.19, probability = 0.31; Fig. 7D). Two older populations have an average age of 275 Ma (20 analyses) and 282 Ma (13 analyses). Zircons from rhyolite (GC-PG-23) are also euhedral with clear oscillatory zoning. The crystals gave concordant intercept age of 272.6 ± 1.6 Ma (16 out of 20 analyses; Fig. 7E).

Thirty-three zircons from four different samples (GC-PG-10, GC-PG −14, GC-PG-18, and GC-PG −23) from the Pha Gnai Prospect were analyzed for Hf isotopes (Table S13, Appendix C). The initial $^{176}Hf/^{177}Hf$ ratios of these samples range from 0.282597 to 0.282856, 0.282441 to 0.282589, 0.282563 to 0.282730, and 0.282603 to 0.282974. The initial εHf values can be grouped into two distinct fields, the positive and negative εHf values ranging from −6. To 12.4 (positive average $\varepsilon Hf_{(t)}$ = 5.8, negative average $\varepsilon Hf_{(t)}$ = -2.7; Fig. 10).

4.2. Zircon trace elements

Zircon trace elements were acquired together with the U/Pb geochronology from the LA-ICPMS analyses (Table 2, Table S14, Appendix D). The anomalous concentration of some trace elements is caused by inclusions within zircon crystal (e.g., apatite). Analyses containing inclusions were excluded using the following criteria: La > 1 ppm, Fe > 5,000 ppm, P > 1,000 ppm, Ti > 50 ppm, and Ba > 8 ppm.

On chondrite-normalized (Sun and McDonough, 1989), REE diagrams the zircon show light rare earth elements (LREE) depletion relative to the heavy rare earth elements (HREE) with positive Ce anomalies. This pattern is typical of zircons worldwide. Most results of the zircons analyzed have similar REE patterns. However, samples from the Phu Kham Deposits (GDD05@19 m), Long Chieng Track Deposits (ACH067 and LSD9@50.9 m), and West of Vientiane site (SM06-114) have anomalously high Ce with relatively either a small or no negative Eu anomaly (Fig. 8).

5. Discussion

5.1. Ages of magmatism

The oldest of the twenty-one LA-ICP-MS zircon U-Pb ages are Early Silurian to Early Devonian (434.9–411.4 Ma) from an area west of Vientiane along Me Khong (WVM), Phu Kham, Ang Noi, and the Long Chieng Track. The earliest of these, a rhyolite from the WVM (SM06-120), crystallized in the Early Silurian (434.9 ± 2 Ma) while the granites were emplaced between the Late Silurian to Early Devonian (425–411 Ma). These are located in an area between the TSFB and LFB (Phu Kham, Long Chieng Track) and are similar in age and characteristics to the late Paleozoic granitic rocks occurring further south in the LFB in Thailand (Bunopas, 1981; Intasopa and Dunn, 1994; Khositanont et al., 2013). Unlike previous studies in Thailand (Gibson, 2009; Khositanont et al., 2013; Shi et al., 2021) Ordovician magmatic or xenocryst zircons were not identified in this study, suggesting that Ordovician magmatism did not extend as far as Laos.

The majority of the granitic and volcanic rocks analyzed in this study formed during the Early to Middle Permian, suggesting widespread magmatism during this period in both the LFB and TSFB.

The youngest samples, from three different locations, including the area west of Vientiane along the Mekong River, Nhon Nhang, and Ban Nape, indicate crystallization ages during the Late Permian to Early Triassic (253–244 Ma). Magmatism from this time period is widespread both in the LFB and TSFB (Hou et al., 2019; Kamvong et al., 2014; Khin Zaw et al., 2014; Khin Zaw and Meffre, 2007; Ouyang et al., 2019; Salam et al., 2014; Sanematsu et al., 2011; Shi et al., 2021; Wang et al., 2023)

Table 2
Zircon trace elements and trace element ratios average values.

Samples	U-Pb ages	Ti	Hf	Y	Zr	Nb	La	Ce	Eu	Th	U	Th/U	$(Eu/Eu^*)_n$	$(Ce/Ce^*)_n$	Ce/Nd	ΔFMQ	Temp (Ti in zircon)
	Ma	ppm	ppm	ppm	ppm	ppm	ppm	ppm	ppm	ppm	ppm						(°C)
GC09-L37	244	2.5	16,408	248	484,202	3.8	0.6	2.7	0.5	7	646	0.0	0.5	1.9	2.1	−3.6	645
SM06-114	244	8.0	7263	2110	486,362	3.0	0.1	51.5	5.8	1144	698	1.5	0.8	66.2	7.5	1.5	757
GC09-L20	253	4.5	12,322	3521	478,484	5.7	0.02	11.1	1.1	187	857	0.4	0.2	126.0	7.6	−0.4	695
GC-PG-18	267	4.7	9130	2548	484,472	4.4	0.02	19.6	1.5	713	620	1.1	0.2	151.6	18.6	0.5	708
GC-PG-23	273	6.1	9191	1943	485,621	2.6	1.9	18.9	0.8	315	289	0.8	0.2	69.4	16.3	0.5	730
GC-PG-14	273	6.6	10,130	1382	486,131	2.8	0.1	14.4	1.0	165	200	0.8	0.5	126.0	16.0	0.7	734
LSD9 @ 50.9 *m*	277	5.5	9919	974	486,986	2.5	0.03	21.6	0.8	654	686	0.9	0.4	110.7	13.5	0.6	714
XSD04@103.8 *m*	279	6.6	9676	1583	486,197	2.8	4.1	23.6	0.5	344	378	0.8	0.2	65.1	10.9	0.6	735
PSD24@54.2 *m*	284	4.3	10,233	1352	486,119	2.0	2.0	15.3	0.8	366	559	0.7	0.2	107.3	8.6	0.2	691
GC-PG-11	285	8.2	9556	1515	486,821	1.5	0.03	9.2	0.8	267	365	0.7	0.3	54.4	8.3	−0.4	751
GC-PG-10	287	7.2	10,216	1373	486,520	1.7	0.4	12.4	0.5	232	294	0.8	0.2	61.9	14.9	0.1	736
HSD01@63.8 *m*	287	3.0	9356	759	487,743	1.8	6.2	16.5	0.3	279	459	0.6	0.2	88.7	24.9	0.7	671
XSD06@100.8 *m*	289	4.0	9597	1137	485,679	2.1	11.4	29.3	0.5	219	329	0.6	0.2	32.0	12.3	1.1	692
ACH067	292	5.2	8127	1341	486,048	1.9	0.06	19.9	1.1	430	500	0.8	0.4	128.6	15.5	0.7	713
GDD05@19 *m*	300	3.7	10,872	904	486,501	3.1	0.06	29.3	1.2	344	590	0.6	0.6	241.1	27.2	1.4	688
ACH054	411	8.4	12,827	3914	475,814	5.2	0.07	5.2	1.2	169	1032	0.5	0.1	13.3	0.7	−2.7	748
AND1@41.7–41.9 *m*	420	5.8	9624	1730	484,945	3.2	5.2	26.0	0.8	202	302	0.6	0.2	78.6	8.5	0.8	723
ACH053	422	5.8	12,462	3659	478,488	1.7	0.05	2.5	0.3	125	517	0.3	0.1	9.7	1.4	−3.4	722
ACH05/2–2	424	7.7	12,022	4005	477,674	1.6	0.10	1.5	0.1	138	666	0.3	0.0	7.7	1.0	−4.4	751
ACH055	425	5.4	12,391	3119	479,453	1.6	0.08	1.2	0.1	99	475	0.2	0.0	5.4	1.6	−4.5	722
SM06-120	435	2.5	10,653	2387	482,693	5.9	1.1	21.4	0.6	410	820	0.5	0.1	38.6	12.4	1.1	653

and host important mineral deposits in in the region, e.g., porphyry-related Cu-Au skarn, epithermal Au-Ag (Cromie et al., 2006; Guo et al., 2019; Kamvong et al., 2014; Khin Zaw et al., 2014; Leaman et al., 2019; Manaka et al., 2014; Salam et al., 2014).

5.2. Zircon cathodoluminescence images

The zircon CL textures of the samples from this study (Fig. 4) can be placed into two groups:

1. Zircons with weakly zoned or unzoned cores with strongly oscillatory rims, such as GDD05@19 m (Phu Kham), SM06-114 (west of Vientiane), GC09-L20 (Ban Nape) and GC09-L37 (Nhon Nhang);
2. Zircon CL textures characterized by strong oscillatory zonation with no distinctive core, such as SM06-120 (west of Vientiane), XSD04@103.8 m (Ban Phonxai), GC-PG-23 (Pha Gnai), and ACH054).

Previous studies (e.g., Leslie et al., 2022) have noted that zircons from fertile porphyries tend to have more complex CL textures than those from less fertile intrusive rocks with the contrasting CL texture in these zircons caused by changes in crystallization rate and trace element distribution. Using these criteria rocks with zircon CL images in the first group would be considered more prospective.

5.3. Zircon geochemical characteristics

The majority of samples show typical zircon chondrite-normalized rare earth element patterns depleted in light rare earth elements (LREE) and relatively high heavy rare earth elements (HREE) with positive Ce and negative Eu anomalies (Figs. 8 and 11; Belousova et al., 2002). However, dacite porphyry from Phu Kham (GDD05@19 m) (Fig. 8E, Fig. 11) demonstrates REE patterns with positive Ce and no Eu anomalies that are consistent with the signature of oxidized and hydrous melts (Ballard et al., 2002; Lu et al., 2016). Likewise, zircons from a quartz diorite from the Mekong River west of Vientiane (SM06-114), rhyolite porphyry (ACH067), and dacite (LSD09@50 m) from the Long Chieng Track also show a large positive Ce anomaly with a small Eu anomaly (Fig. 8C, G and Fig. 11) suggesting a fertile signature for porphyry mineralization.

5.4. Magmatic oxidation-redox state

To further investigate the oxidation state of the magmas, the ΔFMQ values (fayalite-magnetite-quartz fO_2 buffer; Table 2) were calculated using the oxybarometer method (Loucks et al., 2020, Xie et al., 2023). The data clusters in three distinct groups of analyses, with Permian and Triassic zircons from Phu Kham and Triassic zircons from areas west of Vientiane derived from strongly oxidized magmas, and Silurian zircons from the Phu Kham and Long Chieng Track being derived from strongly reduced magmas. Several different thresholds have been used to discriminate intrusions that are fertile and non-fertile for porphyry deposits s, (e.g., Eu/Eu* >0.4 Ballard et al., 2002; Dilles et al., 2015; Pizarro et al., 2020; Nevolko et al., 2021; Eu/Eu* >0.3, 10,000*(Eu/Eu*)/Y > 1, (Ce/Nd)/Y > 0.01 and lower Dy/Yb < 0.3 (Lu et al., 2016). The dacite porphyry from the Phu Kham and quartz diorite from west of Vientiane have the high Eu/Eu* (>0.5), and low Dy/Yb (<0.2) typical of hydrous magmas which have early amphibole and clinopyroxene crystallization and suppression of plagioclase crystallization (Fig. 9A-D). In contrast, most of the zircons from other magmatic rocks in Laos were characterized by lower Eu/Eu* (<0.5). Zircons from some of the Long Chieng Track and Pha Gnai samples also had high values of Eu/Eu* but have lower ΔFMQ values and are therefore considered less prospective. These analyses are also more scattered on many of the trace element plots and Concordia plots, suggesting that there is a complex inheritance.

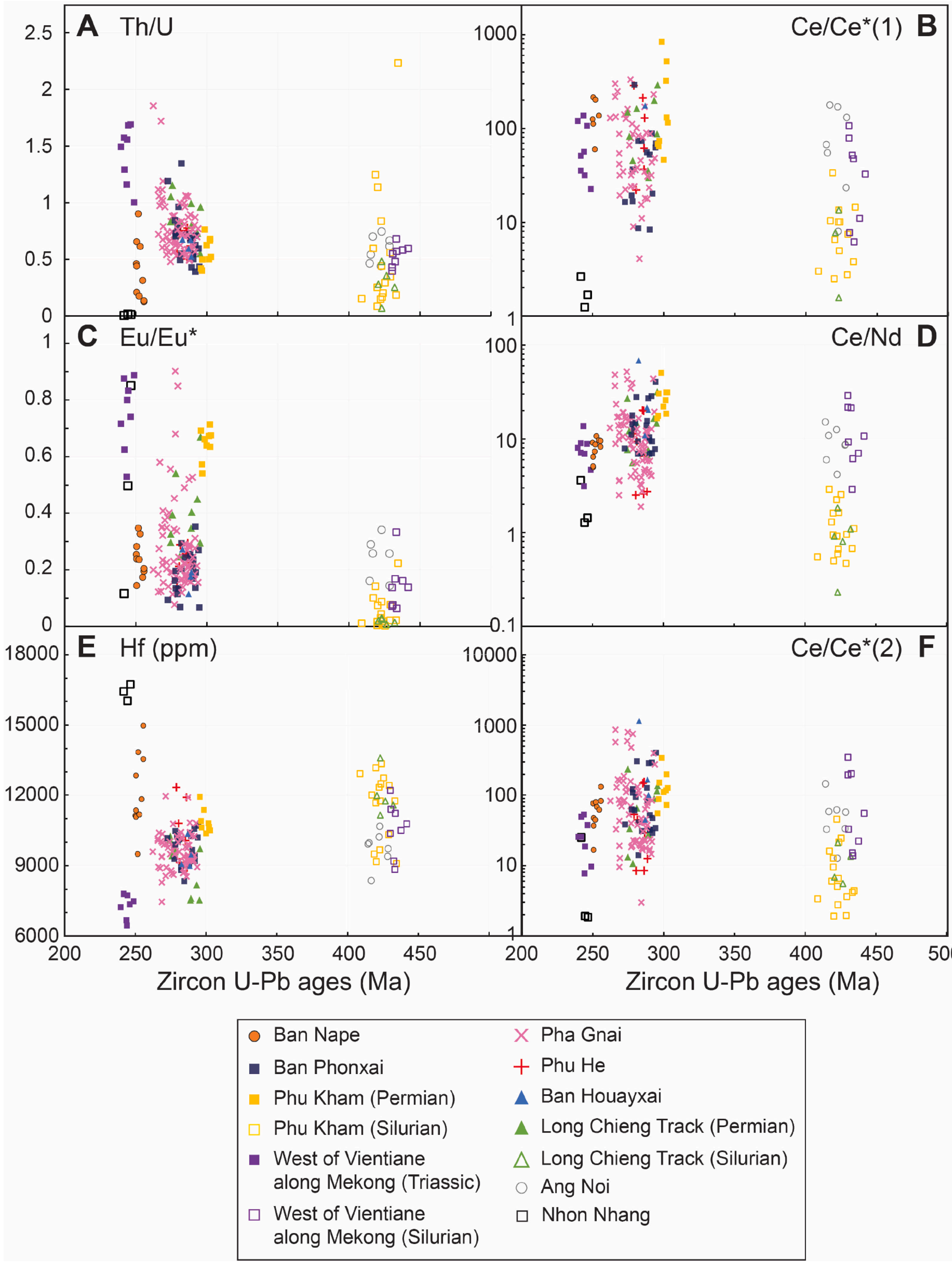

Fig. 11. Zircon Trace element ratios vs U-Pb zircon ages.

5.5. *Zircon crystallization and magmatic fractionation*

Insights into the fractionation history of the zircons can be gained from the Ti and Hf contents with Ti in zircons used to calculate the temperature of crystallization (Ferry and Watson, 2007; Loucks et al., 2020) and Hf to investigate degree of fractionation.

The temperatures obtained by the Ti-in-zircon in this study are low (~650 °C; Fig. 9E and 9G) despite excluding all analyses below detection limit. Similar low temperatures have been reported from other igneous rocks, including mineralized porphyries, and seem to be typical of fluid-fluxed magmatic systems (Chelle-Michou et al., 2014; Leslie et al., 2022; Xie et al., 2023).

Hafnium content in zircon can also be used to illustrate crystallization as crystallizing zircon has a Zr/Hf ratio greater than melt (Lee et al., 2021). The zircons display a negative correlation between Ti-in-zircon calculated temperature and Hf concentration for most of the intrusive suites in this study, suggesting relatively simple and consistent late stage crystallization histories.

5.6. Porphyry Cu fertility relative to magmatic source and age

The geochronology of the zircons analysed in this study demonstrate that the mineral prospects in the LFB and TSFB are associated with three episodes of magmatism: Silurian-Devonian (434–411 Ma), Early to Middle Permian (299–277 Ma), and Late Permian to Middle Triassic (253–243 Ma). The Devonian-Carboniferous (ca 370–310 Ma) which was previously reported (Khin Zaw and Meffre, 2007; Salam et al., 2014; Khin Zaw et al., 2014; Shi et al., 2021; Wang et al., 2020) was not sampled in this study as they may occur in different locations.

The results show that Early to Late Permian (299–250 Ma; Figs. 3-7) magmatism is the dominant magmatic activity associated with epithermal and porphyry mineralization consistent with the previous geochronology (Khin Zaw and Meffre, 2007; Khin Zaw et al., 2014; Shi et al., 2021). The new Hf isotope results show that magmatism during each of the three periods was sourced from both partial melting of the crust and the mantle with both positive and strongly negative εHf values within some samples (e.g., Pha Gnai) and between samples. The magmatic suites (Phu Kham and Long Chieng Track) that have been identified as fertile tend to have much lower Hf at a given temperature than those identified as less fertile for porphyry Cu deposits (Fig. 9G). This suggests fertile magmas tend to be characterized by high εHf values, although some high Hf samples do not have the fertile trace element signature. It is also interesting to note that, according to the U-Pb zircon ages and zircon trace element results (Fig. 9), most of the intrusions that show non-oxidized and anhydrous geochemical characteristics are older (Silurian-Devonian) than the more fertile, oxidized, and hydrous magmas (Permian-Triassic).

6. Conclusions

The geochronological and geochemical characteristics of zircons from LFB and TSFB of northwest Laos were used to evaluate and validate zircon as an indicator of magmatic fertility, especially for the prospectivity of porphyry copper deposits. The main conclusions are as follows:

- The intrusions in the area formed during the Silurian-Devonian (434–411 Ma), Early to Middle Permian (299–277 Ma), and Late Permian to Middle Triassic (253–243 Ma).
- Mantle-derived and crustal contamination signatures in these rocks are related to the history of subduction and arc magmatism in this region.
- The Permo-Triassic magmatic suites from this study are identified to be more fertile than the Silurian-Devonian suites based on their zircon trace element compositions.
- Zircon textures from these rocks can be divided into two groups: 1) zircons with unzoned cores with strongly oscillatory rims and 2) strongly oscillatory zonation with no distinctive cores. The zircons from the first group tend to have trace element characteristics that suggest that they are more fertile, confirming the findings of previous studies.
- The magmatic rocks at Phu Kham, Long Chieng Track and from the area west of Vientiane along the Mekong River have zircons which indicate that these are fertile for porphyry copper deposits, whereas the Pha Gnai and the other magmatic suites have zircons that indicate less fertile magmas.
- This study suggests that zircon as a fertility indicator is a useful tool to distinguish fertile magmatic suites.

CRediT authorship contribution statement

Peerapong Sritangsirikul: Writing – original draft, Visualization, Formal analysis, Data curation, Conceptualization. **Sebastien Meffre:** Writing – review & editing, Supervision. **Khin Zaw:** Writing – review & editing, Supervision. **Ivan Belousov:** Software, Data curation. **Yi-Jen Lai:** Software, Formal analysis, Data curation. **Alex Richards:** Funding acquisition, Conceptualization. **Punya Charusiri:** Writing – review & editing, Funding acquisition.

Declaration of competing interest

The authors declare that they have no known competing financial interests or personal relationships that could have appeared to influence the work reported in this paper.

Data availability

Data will be made available on request.

Acknowledgements

This study has been financially supported by Chulalongkorn University, Department of Mineral Resources (DMR), Thailand and Rio Tinto Exploration (Queensland, Australia). The authors are grateful for the constructive comments of Dr. Jeff Steadman, and the journal reviewers and the Editor-in-Chief for their advice and further suggestions to improve the manuscript.

Appendix A. Supplementary data

Supplementary data to this article can be found online at https://doi.org/10.1016/j.jseaes.2024.106244.

References

Ballard, J.R., Palin, J.M., Campbell, I.H., 2002. Relative oxidation states of magmas inferred from Ce"IV"/Ce"III" in zircon: Application to porphyry copper deposits of northern Chile. Contrib. Miner. Petrol. 144, 347–364. https://doi.org/10.1007/s00410-002-0402-5.

Belousova, E.A., Griffin, W.L., O'Reilly, S.Y., Fisher, N.I., 2002. Igneous zircon: Trace element composition as an indicator of source rock type. Contrib. Miner. Petrol. 143, 602–622. https://doi.org/10.1007/s00410-002-0364-7.

Black, L.P., Kamo, S.L., Allen, C.M., Aleinikoff, J.N., Davis, D.W., Korsch, R.J., Foudoulis, C., 2003. TEMORA 1: A new zircon standard for Phanerozoic U-Pb geochronology. Chem Geol 200, 155–170. https://doi.org/10.1016/S0009-2541(03)00165-7.

Blanchard, S., Rossignol, C., Bourquin, S., Dabard, M.P., Hallot, E., Nalpas, T., Poujol, M., Battail, B., Jalil, N.E., Steyer, J.S., Vacant, R., Véran, M., Bercovici, A., Diez, J.B., Paquette, J.L., Khenthavong, B., Vongphamany, S., 2013. Late triassic volcanic activity in south-east asia: New stratigraphical, geochronological and paleontological evidence from the luang prabang basin (Laos). J Asian Earth Sci 70–71, 8–26. https://doi.org/10.1016/j.jseaes.2013.02.024.

Bounliyong, P., Arribas, A., Watanabe, Y., Echigo, T., Wong, H., 2022. A new orogenic gold belt in Southeast Asia: Geology, mineralogy and genesis of the Vangtat gold deposit. Southeastern Laos. Resource Geology 72. https://doi.org/10.1111/rge.12283.

Bouzari, F., Hart, C.J.R., 2019. Assessing British Columbia porphyry fertility using zircons; in Geoscience BC Summary of Activities 2018: Minerals and Mining. Geoscience BC, Report 2019–1, 45–54.

Bunopas, S., 1981. Paleogeographic history of western Thailand and adjacent part of Southeast Asia—a plate tectonic interpretation. Ph.D. thesis, Victoria University of Wellington, New Zealand. (Reprinted in 1982, Geological Survey paper no. 5, Department of Mineral Resources., Thailand).

Burrett, C., Zaw, K., Meffre, S., Lai, C.K., Khositanont, S., Chaodumrong, P., Udchachon, M., Ekins, S., Halpin, J., 2014. The configuration of Greater Gondwana-Evidence from LA ICPMS, U-Pb geochronology of detrital zircons from the Palaeozoic and Mesozoic of Southeast Asia and China. Gondw. Res. 26, 31–51. https://doi.org/10.1016/j.gr.2013.05.020.

Burrett, C., Udchachon, M., Thassanapak, H., 2021. The truong son, loei-phetchabun, and kontum terranes in Indochina: provenance, rifting, and collisions. Front. Earth Sci. 9, 603565.

Chelle-Michou, C., Chiaradia, M., Ovtcharova, M., Ulianov, A., Wotzlaw, J.F., 2014. Zircon petrochronology reveals the temporal link between porphyry systems and the magmatic evolution of their hidden plutonic roots (the Eocene Coroccohuayco

deposit, Peru). Lithos 198–199, 129–140. https://doi.org/10.1016/J.LITHOS.2014.03.017.
Cromie, P., 2010. Geological setting, geochemistry and genesis of the Sepon gold and copper deposits, Laos (PhD). University of Tasmania, Hobart, Tasmania, Australia.
Cromie, P., Makoundi, C., Zaw, K., Cooke, D.R., White, N., Ryan, C., 2018. Geochemistry of Au-bearing pyrite from the Sepon Mineral District, Laos DPR, Southeast Asia: Implications for ore genesis. J Asian Earth Sci 164, 194–218. https://doi.org/10.1016/j.jseaes.2018.06.014.
Cromie, P.W., Smith, S.G., Codes, U., 2006. New insights through LA-ICP-MS and sulphur isotope investigations into the occurrence of gold in the Sepon gold deposits, Laos. ASEG Extended Abstracts 2006, 1–3. https://doi.org/10.1071/aseg2006ab028.
Dilles, J.H., Kent, A.J., Wooden, J.L., Tosdal, R.M., Koleszar, A., Lee, R.G., Farmer, L.P., 2015. Zircon compositional evidence for sulfur-degassing from ore-forming arc magmas. Econ. Geol. 110 (1), 241–251.
Ferry, J.M., Watson, E.B., 2007. New thermodynamic models and revised calibrations for the Ti-in-zircon and Zr-in-rutile thermometers. Contrib. Miner. Petrol. 154, 429–437. https://doi.org/10.1007/s00410-007-0201-0.
Gardiner, N.J., Searle, M.P., Robb, L.J., Morley, C.K., 2015. Neo-Tethyan magmatism and metallogeny in Myanmar - An Andean analogue? J Asian Earth Sci 106, 197–215. https://doi.org/10.1016/j.jseaes.2015.03.015.
Gardiner, N.J., Robb, L.J., Morley, C.K., Searle, M.P., Cawood, P.A., Whitehouse, M.J., Kirkland, C.L., Roberts, N.M.W., Myint, T.A., 2016a. The tectonic and metallogenic framework of Myanmar: A Tethyan mineral system. Ore Geol Rev 79, 26–45. https://doi.org/10.1016/j.oregeorev.2016.04.024.
Gardiner, N.J., Searle, M.P., Morley, C.K., Whitehouse, M.P., Spencer, C.J., Robb, L.J., 2016b. The closure of Palaeo-Tethys in Eastern Myanmar and Northern Thailand: New insights from zircon U-Pb and Hf isotope data. Gondw. Res. 39, 401–422. https://doi.org/10.1016/j.gr.2015.03.001.
Gardiner, N.J., Hawkesworth, C.J., Robb, L.J., Whitehouse, M.J., Roberts, N.M.W., Kirkland, C.L., Evans, N.J., 2017. Contrasting Granite Metallogeny through the Zircon Record: A Case Study from Myanmar. Sci Rep 7. https://doi.org/10.1038/s41598-017-00832-2.
Gibson, L., 2009. Geology and geochronology of the northern Nan Suture, Thailand (BSc (Hons)). University of Tasmania, Hobart, Tasmania, Australia.
Griffin, W.L., Belousova, E.A., Shee, S.R., Pearson, N.J., O'Reilly, S.Y., 2004. Archean crustal evolution in the northern Yilgarn Craton: U-Pb and Hf-isotope evidence from detrital zircons. Precambr. Res. 231–282. https://doi.org/10.1016/j.precamres.2003.12.011.
Griffin, W.L., Pearson, N.J., Belousova, E.A., Saeed, A., 2006. Comment: Hf-isotope heterogeneity in zircon 91500. Chem Geol 233, 358–363. https://doi.org/10.1016/j.chemgeo.2006.03.007.
Guo, L., Liu, S., Hou, L., Wang, J., Shi, M., Zhang, Q., Nie, F., Yang, Y., Peng, Z., 2019. Fluid Inclusion and H-O Isotope Geochemistry of the Phapon Gold Deposit, NW Laos: Implications for Fluid Source and Ore Genesis. J. Earth Sci. 30, 80–94. https://doi.org/10.1007/S12583-018-0866-5/METRICS.
Hart, M.J.R., Holings, C., Gleeson, P.A., 2017. Assessing the zircon compositional evolution from the Guichon Creek batholith and Highland Valley Copper deposit, south-central BC. Society for Geology Applied to Mineral Deposits (SGA), Extended abstract.
Hawkesworth, C.J., Kemp, A.I.S., 2006. Evolution of the continental crust. Nature 2006 443:7113 443, 811–817. DOI: 10.1038/nature05191.
Hou, L., Xiong, F., Wang, W., Guo, L., Peng, H., Ni, S., Zhang, Q., 2019. Carboniferous-Triassic felsic igneous rocks and typical mineral deposits in the Truong Son orogenic belt, SE Asia: Implications for Paleo-Tethyan tectonic evolution and metallogeny. Ore Geol Rev 112. https://doi.org/10.1016/j.oregeorev.2019.103036.
Hu, F., Wu, F.Y., Wang, J.G., Ducea, M.N., Chapman, J.B., Zaw, K., Lin, W., Sein, K., Meffre, S., 2022. Newly discovered Early Carboniferous and Late Permian magmatic rocks in eastern Myanmar: Implications for the tectonic evolution of the eastern Paleo-Tethys. J Asian Earth Sci 227, 105093. https://doi.org/10.1016/j.jseaes.2022.105093.
Hunyek, V., Sutthirat, C., Fanka, A., 2020. Magma Genesis and Arc Evolution at the Indochina Terrane Subduction: Petrological and Geochemical Constraints From the Volcanic Rocks in Wang Nam Khiao Area, Nakhon Ratchasima. Thailand. Front Earth Sci (lausanne) 8. https://doi.org/10.3389/feart.2020.00271.
Intasopa, S., Dunn, T., 1994. Petrology and Sr-Nd isotopic systems of the basalts and rhyolites, Loei, Thailand. J Southeast Asian Earth Sci 9, 167–180. https://doi.org/10.1016/0743-9547(94)90073-6.
Kamvong, T., 2013. Geology and genesis of porphyry-skarn Cu-Au deposits of the Northern Loei and Truong Son fold belts (PhD). University of Tasmania, Hobart, Tasmania, Australia.
Kamvong, T., Zaw, K., Meffre, S., Maas, R., Stein, H., Lai, C.K., 2014. Adakites in the Truong Son and Loei fold belts, Thailand and Laos: Genesis and implications for geodynamics and metallogeny. Gondw. Res. 26, 165–184. https://doi.org/10.1016/j.gr.2013.06.011.
Khositanont, S., Khin Zaw, Meffre, S., Panjasawatwong, Y., Ouchanum, P., Thanasutihipak, T., 2013. Geotectonic and geochronology of volcano-plutonic rocks in the Loei Phetchabun Fold Belt, in: Senebouttalath, C., Robang, P. (Eds.), Proceedings of the 2nd Lao-Thai Technical Conference on Geology and Mineral Resources. Department of Geology and Minerals, Vientiane, Laos, pp. 81–95.
Leaman, P., Manaka, T., Jarical, K., Villar, M., Libao, J.B., 2019. The geology and mineralization of the Long Chieng Track (LCT) subvolcanic Au-Ag-Cu-Pb-Zn deposit, Lao PDR. Ore Geol Rev. DOI: 10.1016/j.oregeorev.2019.02.010.
Lee, R.G., Byrne, K., D'Angelo, M., Hart, C.J.R., Hollings, P., Gleeson, S.A., Alfaro, M., 2021. Using zircon trace element composition to assess porphyry copper potential of the Guichon Creek batholith and Highland Valley Copper deposit, south-central British Columbia. Miner Depos 56, 215–238. https://doi.org/10.1007/s00126-020-00961-1.
Leslie, C., Meffre, S., Cooke, D.R., Thompson, J., Howard, N., Barker, A., 2022. In: Complex Petrogenesis of Porphyry-Related Magmas in the Cowal District, Australia: Insights from LA ICP-MS Zircon Imaging, in: Tectonomagmatic Influences on Metallogeny and Hydrothermal Ore Deposits. Society of Economic Geologists, pp. 159–180. https://doi.org/10.5382/sp.24.10.
Loader, M.A., Wilkinson, J.J., Armstrong, R.N., 2017. The effect of titanite crystallisation on Eu and Ce anomalies in zircon and its implications for the assessment of porphyry Cu deposit fertility. Earth Planet Sci Lett 472, 107–119. https://doi.org/10.1016/j.epsl.2017.05.010.
Loucks, R.R., Fiorentini, M.L., Henriquez, G.J., 2020. New magmatic oxybarometer using trace elements in zircon. J. Petrol. 61 https://doi.org/10.1093/petrology/egaa034.
Lu, Y.-J., Loucks, R.R., Fiorentini, M., McCuaig, T.C., Evans, N.J., Yang, Z.-M., Hou, Z.-Q., Kirkland, C.L., Parra-Avila, L.A., Kobussen, A., 2016. Zircon Compositions as a Pathfinder for Porphyry Cu $\pm$ Mo $\pm$ Au Deposits, in: Richards, J.P. (Ed.), Tectonics and Metallogeny of the Tethyan Orogenic Belt. DOI: 10.5382/SP.19.13.
Ludwig, K.R., 2012. User's manual for Isoplot 3.75 and 4.15: A geochronological toolkit for Microsoft Excel.
Manaka, T., 2008. Geological setting and mineralization characteristics of the Long Chieng Track and Ban Houayxai deposits, Lao PDR (BSc). University of Tasmania, Hobart, Tasmania, Australia.
Manaka, T., Zaw, K., Meffre, S., Vasconcelos, P.M., Golding, S.D., 2014. The Ban Houayxai epithermal Au-Ag deposit in the Northern Lao PDR: Mineralization related to the Early Permian arc magmatism of the Truong Son Fold Belt. Gondw. Res. 26, 185–197. https://doi.org/10.1016/j.gr.2013.08.024.
Maritati, A., Halpin, J.A., Whittaker, J.M., Daczko, N.R., 2019. Fingerprinting Proterozoic Bedrock in Interior Wilkes Land. East Antarctica. Sci Rep 9. https://doi.org/10.1038/s41598-019-46612-y.
Metcalfe, I., 2011a. Tectonic framework and Phanerozoic evolution of Sundaland. Gondw. Res. 19, 3–21. https://doi.org/10.1016/j.gr.2010.02.016.
Metcalfe, I., 2011b. Palaeozoic-Mesozoic history of SE Asia. Geol Soc Spec Publ 355, 7–35. https://doi.org/10.1144/SP355.2.
Metcalfe, I., 2013. Gondwana dispersion and Asian accretion: Tectonic and palaeogeographic evolution of eastern Tethys. J Asian Earth Sci. https://doi.org/10.1016/j.jseaes.2012.12.020.
Ouyang, Y., Liu, H., Nie, F., Cong, F., Zhang, Jian long, Zhang, Jing hua, Huang, H. xiao, Liu, S. sheng, Lei, C.. yang, 2019. Petrogenesis of Middle Triassic andesite in Sayaburi area, Laos: Constraints from whole-rock geochemistry, zircon U-Pb geochronology, and Sr-Nd isotopes. J Cent South Univ 26, 3502–3515. DOI: 10.1007/s11771-019-4269-2.
Qian, X., Feng, Q., Yang, W., Wang, Y., Chonglakmani, C., Monjai, D., 2015. Arc-like volcanic rocks in NW Laos: Geochronological and geochemical constraints and their tectonic implications. J Asian Earth Sci 98, 342–357. https://doi.org/10.1016/j.jseaes.2014.11.035.
Morley, C.K., Charusiri, P., Watkinson, I.M., 2011. Structural geology of Thailand during the Cenozoic. The Geology of Thailand 273–334. https://doi.org/10.1144/GOTH.11.
Qian, X., Feng, Q., Wang, Y., Chonglakmani, C., Monjai, D., 2016a. Geochronological and geochemical constraints on the mafic rocks along the Luang Prabang zone: Carboniferous back-arc setting in northwest Laos. Lithos 245, 60–75. https://doi.org/10.1016/j.lithos.2015.07.019.
Qian, X., Feng, Q., Wang, Y., Yang, W., Chonglakmani, C., Monjai, D., 2016b. Petrochemistry and tectonic setting of the Middle Triassic arc-like volcanic rocks in the Sayabouli area, NW Laos. J. Earth Sci. 27, 365–377. https://doi.org/10.1007/s12583-016-0669-5.
Qian, X., Wang, Y., Zhang, Y., Wang, Y., Gan, C., Wang, Y., Udchachon, M., Senebouttalath, V., 2021. Constraints of Late Triassic mafic-felsic volcanic rocks in northwestern Laos on the Eastern Paleotethyan post-collisional setting. J Asian Earth Sci 218, 104889. https://doi.org/10.1016/J.JSEAES.2021.104889.
Rezeau, H., Moritz, R., Wotzlaw, J.F., Hovakimyan, S., Tayan, R., 2019. Zircon petrochronology of the Meghri-Ordubad pluton, Lesser caucasus: Fingerprinting igneous processes and implications for the exploration of porphyry Cu-Mo deposits. Econ. Geol. 114, 1365–1388. https://doi.org/10.5382/econgeo.4671.
Rossignol, C., Bourquin, S., Poujol, M., Hallot, E., Dabard, M.P., Nalpas, T., 2016. The volcaniclastic series from the Luang Prabang Basin, Laos: A witness of a triassic magmatic arc? J Asian Earth Sci 120, 159–183. https://doi.org/10.1016/j.jseaes.2016.02.001.
Salam, A., 2013. Geological, geochemical and metallogenic study of the Chatree epithermal deposit, Phetchabun Province, Central Thailand (PhD). University of Tasmania, Hobart, Tasmania, Australia.
Salam, A., Zaw, K., Meffre, S., McPhie, J., Lai, C.K., 2014. Geochemistry and geochronology of the Chatree epithermal gold-silver deposit: Implications for the tectonic setting of the Loei Fold Belt, central Thailand. Gondw. Res. 26, 198–217. https://doi.org/10.1016/j.gr.2013.10.008.
Sanematsu, K., Murakami, H., Duangsurigna, S., Vilayhack, S., Duncan, R.A., Watanabe, Y., 2011. 40Ar/39Ar ages of granitoids from the Truong Son fold belt and Kontum massif in Laos. J. Mineral. Petrol. Sci. 106, 13–25. https://doi.org/10.2465/jmps.091216.
Shen, P., Hattori, K., Pan, H., Jackson, S., Seitmuratova, E., 2015. Oxidation Condition and Metal Fertility of Granitic Magmas: Zircon Trace-Element Data from Porphyry Cu Deposits in the Central Asian Orogenic Belt. Econ. Geol. v.
Shi, M., Khin, Z., Liu, S., Xu, B., Meffre, S., Cong, F., Nie, F., Peng, Z., Wu, Z., 2021. Geochronology and petrogenesis of Carboniferous and Triassic volcanic rocks in NW Laos: Implications for the tectonic evolution of the Loei Fold Belt. J Asian Earth Sci 208. https://doi.org/10.1016/j.jseaes.2020.104661.

Shu, Q., Chang, Z., Lai, Y., Hu, X., Wu, H., Zhang, Y., Wang, P., Zhai, D., Zhang, C., 2019. Zircon trace elements and magma fertility: insights from porphyry (-skarn) Mo deposits in NE China. Miner Depos. https://doi.org/10.1007/s00126-019-00867-7.

Sláma, J., Košler, J., Condon, D.J., Crowley, J.L., Gerdes, A., Hanchar, J.M., Horstwood, M.S.A., Morris, G.A., Nasdala, L., Norberg, N., Schaltegger, U., Schoene, B., Tubrett, M.N., Whitehouse, M.J., 2008. Plešovice zircon - A new natural reference material for U-Pb and Hf isotopic microanalysis. Chem Geol 249, 1–35. https://doi.org/10.1016/j.chemgeo.2007.11.005.

Sone, M., Metcalfe, I., 2008. Parallel Tethyan sutures in mainland Southeast Asia: New insights for Palaeo-Tethys closure and implications for the Indosinian orogeny. Comptes Rendus - Geoscience 340, 166–179. https://doi.org/10.1016/j.crte.2007.09.008.

Wang, D., Lin, F., Shi, M., Wang, H., Yang, X., 2023. Geological setting, tectonic evolution and spatio-temporal distributions of main mineral resources in South East Asia: A comprehensive review. Solid Earth Sciences. https://doi.org/10.1016/j.sesci.2022.12.003.

Wang, S., Mo, Y., Wang, C., Ye, P., 2016. Paleotethyan evolution of the Indochina Block as deduced from granites in northern Laos. Gondw. Res. 38, 183–196. https://doi.org/10.1016/j.gr.2015.11.011.

Wang, Y., Qian, X., Cawood, P.A., Liu, H., Feng, Q., Zhao, G., Zhang, Y., He, H., Zhang, P., 2018. Closure of the East Paleotethyan Ocean and amalgamation of the Eastern Cimmerian and Southeast Asia continental fragments. Earth Sci Rev 186, 195–230. https://doi.org/10.1016/j.earscirev.2017.09.013.

Wang, Y., Wang, Y., Qian, X., Zhang, Y., Gan, C., Senebouttalath, V., Wang, Y., 2020a. Early Paleozoic subduction in the Indochina interior: Revealed by Ordo-Silurian mafic-intermediate igneous rocks in South Laos. Lithos 362–363. https://doi.org/10.1016/j.lithos.2020.105488.

Wang, Y., Yang, T., Zhang, Y., Qian, X., Gan, C., Wang, Y., Wang, Y., Senebouttalath, V., 2020b. Late Paleozoic back-arc basin in the Indochina block: Constraints from the mafic rocks in the Nan and Luang Prabang tectonic zones. Southeast Asia. J Asian Earth Sci 195. https://doi.org/10.1016/j.jseaes.2020.104333.

Wiedenbeck, M., Alle, P., Corfu, F., Griffin, W.L., Meier, M., Oberli, F., Quadt, A.V., Roddick, J.C., Spiegel, W., 1995. Three natural zircon standards for U-Th-Pb, Lu-Hf, trace element and REE analyses. Geostand. Newslett. 19, 1–23. https://doi.org/10.1111/j.1751-908X.1995.tb00147.x.

Xie, F., Tang, J., Jia, M., Lang, X., Sun, Y., He, Y., Liu, J., 2023. Zircon and apatite fingerprints on the magma fertility for the Jurassic igneous rocks in the southern Lhasa subterrane. Tibet. Ore Geol Rev 161. https://doi.org/10.1016/j.oregeorev.2023.105662.

Zaw, K., 2021. Tectonic, geochronological and metallogenic framework of ore deposits along Loei Fold Belt, Laos PDR and Thailand: Extension into Myanmar and Cambodia. Special Talk, 4th International Virtual Conference on Substantial Scientific Collaboration of Ocean and Earth Science between Myanmar and China.

Zaw, K., Meffre, S., Lai, C.K., Burrett, C., Santosh, M., Graham, I., Manaka, T., Salam, A., Kamvong, T., Cromie, P., 2014. Tectonics and metallogeny of mainland Southeast Asia - A review and contribution. Gondw. Res. 26, 5–30. https://doi.org/10.1016/j.gr.2013.10.010.

Zaw, K., Meffre, S., Burrett, C., Shi, M., Hu, F., Lai, C.-K., 2022a. Recent advances in studies of tectonics and metallogeny of Loei and Truong Son Fold Belts in SE Asia. In: Keynote Address, 6th GEOINDO 2022, the International Conference on Geology, Geotechnology, and Mineral Resources of Indochina. Khon Kean University, Thailand, pp. 13–15.

Zaw, K., Meffre, S., Salam, A., 2022b. Geochronological and metallogenic framework of ore deposits along Loei Fold Belt, Laos PDR and Thailand: Extension into Myanmar and Cambodia. In: Proceeding of Earth Resources and Geo-Environment Technology (EraGET). Phnom Penh, Cambodia, pp. 7–13.

Zaw, K., Meffre, S., higher degree students,, 2007. Metallogenic relations and deposit scale studies, final report: geochronology, metallogenesis and deposit styles of Loei Fold Belt in Thailand and Laos PDR. University of Tasmania, Hobart.

Zhang, Z., Shu, Q., Wu, C., Zaw, K., Cromie, P., von Dollen, M., Xu, J., Li, X., 2020. The endogenetic metallogeny of northern Laos and its relation to the intermediate-felsic magmatism at different stages of the Paleotethyan tectonics: A review and synthesis. Ore Geol Rev. https://doi.org/10.1016/j.oregeorev.2020.103582.

Zou, H., Han, R., Liu, M., Cromie, P., Zaw, K., Fang, W., Huang, J., Ren, T., Wu, J., 2020. Geological, geophysical, and geochemical characteristics of the Ban Kiouchep Cu–Pb–Ag deposit and its exploration significance in Northern Laos. Ore Geol Rev 124. https://doi.org/10.1016/j.oregeorev.2020.103603.

Zou, X.Y., Qin, K.Z., Han, X.L., Li, G.M., Evans, N.J., Li, Z.Z., Yang, W., 2019. Insight into zircon REE oxy-barometers: A lattice strain model perspective. Earth Planet Sci Lett 506, 87–96. https://doi.org/10.1016/j.epsl.2018.10.031.